의학박사 학위논문

Microglial STAT3-mediated neuron-microglia interactions in major depressive disorder

우울증에서 미세아교세포 STAT3 에 의해 매개되는 신경-미세아교세포 상호작용

2019 년 2 월

서울대학교 대학원 의과학과

약리학전공

권 순 호

A thesis of the Degree of Doctor of Philosophy

우울증에서 미세아교세포 STAT3 에 의해 매개되는 신경-미세아교세포 상호작용

Microglial STAT3-mediated neuron-microglia interactions in major depressive disorder

February 2019

The Department of Biomedical Science,

(Major in Pharmacology)

Seoul National University

College of Medicine

Sun-Ho Kwon

ABSTRACT

Neuron–microglia interactions play a crucial role in maintaining the neuroimmune system. The balance of neuroimmune system has emerged as an important process in the pathophysiology of depression. However, how neuron–microglia interactions contribute to major depressive disorders has been poorly understood. Herein, I demonstrated that microglia–derived neuronal changes induced antidepressive–like behavior by using microglia–specific signal transducer and activator of transcription 3 (STAT3) knockout ($STAT3^{fl/fl}$;LysM–$Cre^{+/-}$) mice. I found that microglia–specific STAT3 knockout mice showed antidepressive–like behavior in the forced swim, tail suspension, sucrose preference and open field tests. Surprisingly, the secretion of macrophage colony–stimulating factor (M–CSF) was increased from neuronal cells in the brains of $STAT3^{fl/fl}$;LysM–$Cre^{+/-}$ mice. Moreover, the phosphorylation of antidepressant–targeting mediators and brain–derived neurotrophic factor (BDNF) expression were increased in the brains of $STAT3^{fl/fl}$;LysM–$Cre^{+/-}$ mice as well as in neuronal cells in response to M–CSF stimulation. Collectively, microglial STAT3 regulates depression–related behaviors via M–CSF–mediated neuronal activity, suggesting that inhibition of microglial STAT3 might be a new

therapeutic strategy for depression.

Keywords: STAT3, M-CSF, microglia, neuron-microglia interactions, major depressive disorder, neuronimmune system

Student number: 2013-21765

CONTENTS

LIST OF TABLES AND FIGURES

LIST OF ABBREVIATIONS

STAT3: Signal transducer and activator of transcription 3

M-CSF: Macrophage colony-stimulating factor

GSK3β : glycogen synthase kinase-3β

ERK1/2: Extracellular signal-regulated kinase 1/2

BDNF: Brain-derived neurotrophic factor

MDD: Major depressive disorder

GFAP: Glial fibrillary acidic protein

Iba-1: Ionized calcium binding adaptor molecule 1

CCL2: Chemokine C-C motif ligand 2

ELISA: Enzyme-linked immunosorbent assay

ANOVA: Analysis of variance

INTRODUCTION

Microglia are the resident macrophages of the central nervous system (CNS), belonging to the glial system of non-neuronal cells that support and protect neuronal functions in the brain and the spinal cord (Lawson et al, 1990). Microglia arise during the early embryonic life, accounting for 10-20% of the total glial cell population within the CNS parenchyma. Regulation of the microglial function plays a pivotal role in maintaining the homeostasis of the CNS in both health and disease (Perry et al, 2010).

Microglia are immune cells that act as a sentinel to detect the first signs of pathogenic invasion or tissue damage in the brain's sensitive immune system (Wake et al, 2013). Under the inflammatory conditions of an active immune response, microglia regulate the potential damage to the CNS and supports tissue repair and remodeling. Abnormal activation of microglia and microglia-induced inflammation are observed in a variety of brain pathologies, suggesting that microglia have a direct effect on neurons and contributes to disease progression (Yirmiya and Goshen, 2011).

Neuron–microglia interactions play a crucial role in maintaining the neuroimmune system (Rogers et al, 2011; Wake et al, 2013; Zhan et al, 2014). Recent evidence has focused on the imbalance of the neuroimmune system in association with psychiatric disorders, such as major depression (Couch et al, 2013). Presumably, microglial dysfunction causes disturbances in synaptic regulation, resulting in major depression. However, the cellular and molecular mechanisms of major depression underpinning the bidirectional interplay between neurons and microglia remain unclear.

For decades, many studies focused on novel therapeutic approaches for major depression (Domino et al, 2008; Goodyer et al, 2007). The intracellular signaling pathways of extracellular signal–regulated kinase (ERK)1/2, Akt and glycogen synthase kinase–3 beta (GSK3β) have been identified as the potent targets for antidepressants (Duman et al, 2016). According to postmortem studies, ERK1/2 signaling, which is downregulated in the brains of patients with major depression (Dwivedi et al, 2005; Dwivedi et al, 2001), has been implicated in antidepressant treatment (Duman et al, 2012b; Einat et al, 2003; Tardito et al, 2006). While the blockade of the ERK signaling pathway leads to depression–related behaviors, antidepressant treatments increase ERK phosphorylation (Gourley et al, 2007; Hisaoka et al, 2007). Additionally,

GSK3β is regarded as a key factor involved in psychiatric diseases (Beurel et al, 2015; Chuang et al, 2011; Jope and Roh, 2006). Recent studies showed increased GSK3β activity in the cortical regions of postmortem brains of suicide victims who had suffered from depression (Karege et al, 2007). However, the inactivation of GSK3β using lithium or valproate may alleviate unipolar depression (Chen et al, 2000; Cipriani et al, 2006; Davis et al, 1996). GSK3β is also negatively regulated by phosphatidylinositol 3-kinase (PI3K)-mediated Akt activation (Fang et al, 2000).

Despite having a sufficient knowledge of ERK1/2 and Akt/GSK3β signaling pathways, the etiological factors leading to major depression remain unknown. Recent studies showed that neuroinflammation caused by stress-induced activation of microglia leads to depressive-like behaviors (Brites and Fernandes, 2015; Steiner et al, 2011; Streit et al, 2004). In addition to microglial activation, microglial senescence and decline can negatively affect neurogenesis, causing major depression (Caldeira et al, 2014; Kreisel et al, 2014). These findings suggest the importance of microglial activation status in depression.

Signal transducer and activator of transcription 3 (STAT3) is activated by various cytokines and growth factors, and plays a major role in

causing an inflammatory response by increasing cell activation. STAT3 also functions as one of the transcription factors for cytokine production (El Kasmi et al, 2006), such as soluble intracellular cell adhesion molecule-1 (sICAM-1) (Park et al, 2013), interleukin-6 (IL-6) (Mori et al, 2011), interleukin-10 (IL-10) (Riley et al, 1999), tumor necrosis factor-alpha (TNF-α) (Chabot et al, 1997; Riazi et al, 2008) and interleukin-1 beta (IL-1β) (Clausen et al, 2008). Increased these cytokines can confer protection to the brain following an acute inflammation, yet under conditions of chronic immune activation, microglia become a main source of inflammatory cytokines that can affect the neuronal function and neurotransmitter system (Felger and Lotrich, 2013; Khairova *et al*, 2009). These cytokines also have been identified as mediators for the neuroimmune system of depression (Hodes et al, 2015). For example, pathological levels of these cytokines contribute to behavioral deficits such as depressive-like behavior (Audet and Anisman, 2013; Khairova *et al*, 2009; Schiepers *et al*, 2005), requiring a more sophisticated manipulation of cytokine levels. Thus, by inhibiting STAT3, the level of mediators affecting the inflammatory response can be reduced, which has been selected as a therapeutic target for psychiatric diseases as well as various inflammatory diseases.

In this study, I hypothesized that STAT3 signaling in microglia affects

neuron–microglia interactions via secreted cytokines, resulting in synaptic and behavioral changes. To investigate the key factors regulated by microglial STAT3 in neuron–microglia interactions, I used microglia-targeted STAT3–deficient mice and analyzed the molecular mechanisms and their behavioral phenotypes. As a result, I revealed that STAT3 dysfunction in microglia led to antidepressive–like behavior via crosstalk between neurons and microglia, suggesting a novel therapeutic avenue for major depression.

MATERIALS AND METHODS

Experimental animals and genotyping

Mice homozygous for the loxP-flanked (floxed) STAT3 gene ($STAT3^{fl/fl}$) were kindly gifted from Dr. S. Akira (Osaka University, Suita, Japan). Mice carrying a Cre transgene under the control of the distal LysM promoter ($LysM-Cre^{+/+}$) were purchased from the Jackson Laboratory (Bar Harbor, ME, USA). Mice with a STAT3 deletion in myeloid cells were generated by crossing mice with the floxed STAT3 allele with mice expressing Cre under the control of the LysM promoter. Genomic DNA was isolated from tail tips using a NucleoSpin genomic DNA purification kit (Macherey-Nagel GmbH & Co., Duren, North Rhine-Westphalia, Germany). The polymerase chain reaction (PCR) was performed using AccuPower™ PCR premix (Bioneer, Daejeon, Korea) with the primers, which are specific for exons 22 and 23 of STAT3 and Cre transgene, according to the manufacturer's instructions. All experiments were performed with male mice aged 8 – 10 weeks. Experimental animals were maintained under specific pathogen-free conditions and 22±1° C with a reversed 12-hour light-dark cycle (lights on at 7:00 AM). All experimental procedures were reviewed and approved by the Institutional Animal Care and Use Committee (IACUC) at the College of

Medicine, Seoul National University.

Primary microglia cell culture

Primary microglia cells were isolated from primary mixed glial cells of 2-day-old mice. To obtain mixed glial cells, cerebral cortices were dissected, carefully stripped of their meninges, and dissociated into a single-cell suspension by trituration. Cells were cultured on poly-L-lysine (Sigma-Aldrich, St Louis, MO, USA)-coated 100mm^2 culture dish in Dulbecco's modified Eagle's medium (DMEM, Hyclone, Logan, UT, USA) containing 10% fetal bovine serum (FBS) and 1% penicillin-streptomycin solution (Gibco, Grand Island, NY, USA), and incubated at 37° C in 5% CO_2. On the third day of culture, cells were vigorously washed with pipetting and the media was replaced to remove debris. After six days *in vitro*, cells were transferred to a T-75 flask and incubated for 1-3 weeks. Then, the conditioned media were replaced with fresh media to achieve complete confluence. To isolate microglia, the T-75 flask was rotated (200rpm, 37° C, 5 hours) using a temperature-controlled, non-humidified shaker, and then supernatant media containing microglia was centrifuged (215×g, 5 minutes). The microglial pellet was suspended and seeded onto poly-L-lysine-coated 60 mm^2 cover glass bottom dish (SPL Life Sciences, Pocheon, Korea), and incubated at 37° C in 5% CO_2.

Cell culture and co-culture experiments

Mouse microglia cell line BV2 and mouse hippocampal neuronal cell line HT22 (ATCC, Manassas, VA, USA) were cultured in DMEM containing 10% FBS and 1% penicillin-streptomycin solution and incubated at 37° C in 5% CO_2. HT22 cells were starved before stimulation for 8 hours and then stimulated with M-CSF (40ng/ml, ProSpec, East Brunswick, NJ, USA) in a time-dependent manner or 24 hours. Before the co-culture experiment, BV2 cells were seeded in 6-well dishes at 4×10^4 cells/well and transfected with STAT3 siRNAs for 24 hours. The cells were washed twice with PBS and then incubated in fresh DMEM containing 10% FBS after transfection. Then, the HT22 cells were cultured on 0.4μm pore-size Falcon cell culture inserts (Corning Incorporated, Durham, NC, USA) at 2×10^5 cells/well in DMEM containing 10% FBS and co-cultured with BV2 cells for 24 hours. To confirm the effect of macrophages on neurons, HT22 cells were treated with culture medium of RAW264.7 cells with or without STAT3 inhibition for 24 hours.

siRNA transfection

BV2 cells and RAW264.7 cells were cultured in the growth condition to a density of 2×10^5 cells in 6-well culture plate. The cells were transfected

with the siRNAs using HiperFect transfection reagent (Qiagen, Germantown, MD, USA) according to the fast-forward protocol of manufacturer's instructions. STAT3 siRNAs targeting two different regions of STAT3 (SI01435287 and SI01435294), and a negative control siRNA (1027280) were purchased from Qiagen.

Immunohistochemistry

Brains of mice were perfused with buffer containing 4% paraformaldehyde, fixed for two days in 4% paraformaldehyde at 4° C and embedded in paraffin. The paraffin blocks were cut using a microtome (4 μm, Finesse E +, Thermo Shandon, Runcom, UK). Paraffin slices were mounted on the silane-coated micro slides (Muto Pure Chemicals, Tokyo, Japan), and then allowed to air dry at room temperature in the dark for 24 hours. Before immunostaining, the slides were deparaffinized in xylene, dehydrated through graded alcohols, and heated in citrate buffer for 10 minutes. Nonspecific binding was blocked with 5% normal goat serum (Vector Laboratories, Burlingame, CA, USA) in PBS. For immunocytochemistry, cells were grown on a poly-L-lysine-coated 60mm^2 cover glass bottom dish for 24 hours and rinsed with PBS at room temperature. Then, the cells were fixed with 4% paraformaldehyde for 10 minutes and permeabilized in 0.1% Triton X-100. Nonspecific binding was blocked with 1% bovine serum albumin

(Bovogen, East Keilor, VIC, AUS) in PBS. The fluorescent immunostaining was performed with the primary antibodies for p-STAT3 (1:200; Cell Signaling Technology, MA, USA), STAT3 (1:200; Abcam, Cambridge, UK), Iba-1 (1:200; Wako, Japan), Iba-1 (1:200; Novus Biologicals, CO, USA), NeuN (1:200; Merck Millipore, MA, USA), and visualized using Cy3 goat anti-mouse IgG, 488 goat anti-mouse IgG, Cy3 donkey anti-rabbit IgG (1:200; BioLegend, CA, USA), 488 donkey anti-rabbit IgG (1:200; Abcam, Cambridge, UK) and 488 bovine anti-goat IgG (1:200; Santa Cruz Biotechnology, CA, USA). The slides were mounted with 4',6-diamidino-2-phenylindole (DAPI), and images were collected using the LSM510 program on a confocal microscope (Carl Zeiss MicroImaging, Inc., München, Germany).

Restraint stress procedure

Mice were transferred to a behavior analysis test room before initiating chronic stress procedures. For the chronic stress, the experimental group was immobilized in a rodent restrainer (Ø, 30×95mm) and separated from the control group for the duration (2 hours a day for 14 consecutive days). After the chronic restraint stress, the mice were returned to their home cages for a day, and then behavioral experiments were conducted.

Behavioral experiments

Behavioral experiments were performed independently according to the behavioral test paradigm, and separate groups were used for each behavioral test paradigm. Experimental mice were subjected to tail suspension and forced swimming tests at intervals of one day after 14 days of chronic restraint stress to assess despair-based behavior. A separate cohort of mice was used to conduct sucrose preference test to assess reward-based behavior under normal and chronic stress conditions. Another group was used to assess behavior based on anxiety and locomotion, the following series of behavioral experiments were conducted at intervals of two days: handling, elevated plus maze test, open field test, and rotarod test. All mice were sacrificed immediately after the behavioral experiment, and all brain tissues of the mice used in the behavioral experiments under chronic restraint stress were extracted.

Forced swim test

The forced swim test was performed as described previously (Page et al, 1999). Briefly, mice were placed in a glass beaker (2L beaker) which was filled to a depth of 18 cm with water (25° C). The water was regularly changed between subjects. The duration of immobility was recorded and measured with a video camera for 6 minutes.

Tail suspension test

Mice were suspended by their tails from a steel bar using adhesive tape in a chamber with opaque walls. The distance between the floor of the chamber and the steel bar was approximately 40cm. Mice that climbed onto their tails or fell off during the test were excluded from analyses. Mice movements were videotaped for 6 minutes, and the total duration of immobility recorded.

Sucrose preference test

The sucrose preference test was conducted as described previously (Strekalova et al, 2004). After food and water deprivation for 24 hours, mice were given free access to both water and 1% sucrose solution in individual cages for 24 hours. The position of each bottle was switched after 12 hours to rule out side preference. The consumption of water and sucrose solution was measured by weighing the bottles. The preference for sucrose solution was calculated as a percentage of the volume of consumed sucrose solution over the total volume of liquid drunk.

Open field test

Mice were placed in the center of an open field box (40×40×40cm), illuminated by the light of 20 lx intensity and the mice movements were recorded with a video camera for 30 minutes. The total distance traveled and time spent in the center of the entire open field (20×20cm) were

calculated using video tracking software (EthoVision XT 8.5, Noldus, USA).

Elevated plus maze test

The elevated plus maze consisted of two open arms (30×5cm) and two closed arms of the same size, with 15cm high side walls. The four arms and central square were 50cm above the ground. Mice were placed in the central square of the maze (5×5cm), facing the open arms. The mice movements were recorded during a 5-minutes test period. The number of entries, the time spent in the open and closed arms were calculated using video tracking software (EthoVision XT 8.5, Noldus, USA).

Rotarod test

The rotarod test was performed by a coordination test system (Rotamex 5, Columbus Ins, USA). The mice were placed on a rotating rod (3cm in diameter) accelerated from 3 to 50rpm for 6 minutes.

Cytokine array and enzyme-linked immunosorbent assay (ELISA)

The expression of cytokines and chemokines in the culture supernatant was assessed with a mouse cytokine antibody array panel A (R&D Systems, MN, USA) according to the manufacturer's instructions. Total M-CSF in the conditioned medium of the cultured cells was measured

using the quantikine ELISA kit (R&D Systems, MN, USA) according to the manufacturer's instructions. The data were presented as absorbance units at 450 nm and correction absorbance units at 540 nm from three independent experiments.

RNA isolation and quantitative real-time PCR

Total RNA was isolated from BV2 and HT22 cells using an RNAiso Plus reagent (Takara, Shiga, Japan) and cDNA was synthesized using ReverTra Ace qPCR RT Master Mix (TOYOBO, Osaka, Japan). Quantitative real-time PCR was performed using the EvaGreen qPCR Mastermix (Applied Biological Materials, Richmond, Canada), and the results were normalized to the signals of GAPDH expression. Primers for CCL2 (QT00167832), STAT3 (QT00148750), ICAM-1 (QT00155078), TNF-α (QT00104006), IL-1β (QT01048355), IL-6 (QT00098875), IL-10 (QT00106169), M-CSF (QT01164324) and GAPDH (QT01658692) were purchased from Qiagen.

Western Blot

Cells were washed with the cold PBS, and then lysed in the triton lysis buffer containing 1% Triton X-100, 50mM Tris-HCl (pH 7.4), 0.35 M NaCl, 0.5% Nonidet P-40, 10% glycerol, 0.1% SDS, 1mM EDTA, 1mM EGTA, 0.2mM Na_3VO_4, 1mM PMSF and 0.5mM NaF. Brain tissue was

homogenized and lysed in the triton lysis buffer. After incubation for 30 minutes on ice, insoluble debris was removed by centrifugation at 16,000×g for 10 minutes at 4° C. The lysates were resolved in sodium dodecyl sulfate polyacrylamide gel electrophoresis (SDS-PAGE) and transferred to nitrocellulose membranes (GE Healthcare, Pittsburgh, PA, USA). The membranes were blocked in 5% skim-milk (LPS solutions, Daejeon, Korea) and probed with the primary antibodies for phospho-STAT3 (Tyr705), STAT3, phospho-ERK1/2 (Thr202 / Tyr204), ERK1/2, phospho-Akt (Ser473), Akt (1:1,000; Cell Signaling Technology, MA, USA), BDNF, phospho-GSK3β (Ser9), GSK3β (1:1,000; Santa Cruz Biotechnology, CA, USA), α-tubulin (1:1,000; Thermo Scientific, Grand Island, NY, USA), VGLUT1, PSD95 (1:2,000; 1:1,000; Synaptic Systems, Göttingen, Germany), Synaptophysin (1:1,000; Epitomics, Burlingame, CA, USA), GFAP (1:1,000; DAKO, CA, USA) and Iba-1 (1:1,000; Novus Biologicals, CO, USA) for the target molecules, followed by HRP-conjugated secondary antibodies for goat anti-mouse IgG, goat anti-rabbit IgG (1:10,000; Enzo Life Science, NY, USA) and donkey anti-goat IgG (1:10,000; Santa Cruz Biotechnology, CA, USA). The membranes were visualized using an ECL detection kit (SurModic Inc., Eden Prairie, MN, USA).

Slice preparation for tissue slice culture

Mice were anesthetized with isoflurane and decapitated, and the brains were immediately removed and placed in ice-cold slicing solution (0-4° C) containing the following artificial cerebrospinal fluid (aCSF): 124mM NaCl, 2.5mM KCl, 1mM NaH_2PO_4, 1.3mM $MgCl_2$, 2.5mM $CaCl_2$, 26.2mM $NaHCO_3$, and 20mM D-glucose, bubbled with a gas mixture of 5% CO_2 / 95% O_2 to maintain a pH of 7.4. Coronal slices containing mPFC were obtained using a Vibratome (slice thickness 250 μm; Leica VT1200S; Leica, Nussloch, Germany). After cutting, the slices were kept for 30 minutes at 35° C and stimulated with M-CSF (10nM) for synaptosomal preparations.

Golgi staining

Dendritic spine density was analyzed using an FD Rapid GolgiStain Kit (FD Neurotechnologies, Baltimore, MD, USA) was used according to the manufacturer's instructions. In brief, mice were anesthetized with isoflurane and decapitated. The brains were immediately removed, rinsed and immersed in the impregnation solution and stored at room temperature for two weeks in the dark. The brains were transferred into a solution containing sucrose and stored at room temperature in the dark for at least three days. Frozen slices of the brain were cut using a freezing microtome (100 μm, Cryotome FE, Thermo Shandon, Runcom, UK). The slices were mounted on gelatin-coated microscope slides and then

allowed to air dry at room temperature in the dark for three days. Slides were then rinsed with distilled water before being dehydrated in absolute alcohol, cleared with xylene, and covered with non-acidic synthetic balsam and cover slips.

Brain synaptosomal preparation

Brain synaptosomal preparation was performed as described previously (Kamat et al, 2014). In brief, the prefrontal cortex was homogenized in 10% (w/v) of 0.32M sucrose-HEPES buffer on ice, and the homogenate was centrifuged at 600×g for 10 minutes at 4-8° C. The HEPES buffer was composed of 145mM NaCl, 5mM KCl, 2mM $CaCl_2$, 1mM $MgCl_2$, 5mM glucose, and 5mM HEPES (pH 7.4). The supernatant was diluted 1:1 with 1.3M HEPES sucrose, to yield a suspension with a final concentration of 0.8M HEPES sucrose. This suspension was further centrifuged at three times with HEPES buffer at 12,000×g for 15 minutes at 4° C. The pellet consisting of synaptosomes was suspended in RIPA buffer (mixed with a protease inhibitor and PMSF) along with 0.2% TritonX-100 and centrifuged at 20,000×g for 30 minutes. The resulting synaptosomes were immediately used for the Western blot.

Statistical analysis

One-way analysis of variance (ANOVA) was used for the statistical

analysis of cytokine array. Multiple comparisons were investigated via Tukey–Kramer's post hoc test. Two–way ANOVA (genotype × stress) was applied to assess behavioral experiments with chronic restraint stress. Bonferroni's post hoc test was performed if applicable. Repeated measures ANOVA (genotype × trial session) was used to analyze locomotive activity and learning and memory. Group comparisons of immunofluorescence intensity, RNA and protein expressions were performed by Student's t–tests. The data were assessed to ensure normality with the Shapiro–Wilk test, and where violations of the normality assumptions were found, non–parametric statistics were conducted. All data are presented in means ± standard error of means (SEM). All statistical analyses were conducted using SigmaPlot software (ver. 13, Systat Software, San Jose, CA, USA).

RESULTS

Targeting STAT3 in microglia by using STAT3$^{fl/fl}$;LysM−Cre$^{+/-}$ mice

Microglia are unique glial cells derived from common myeloid progenitors during developmental stages of the CNS, possibly explaining the experimental paradigm for neuron−microglia interactions. In this study, I targeted STAT3 in microglia, a key transcription factor for immune responses, due to its relevance in the regulation of cytokine expression levels. I employed the myeloid cell−specific STAT3−deficient mouse model by breeding STAT3 floxed mice and LysM−Cre mice. I denoted STAT3$^{wt/fl}$;LysM−Cre$^{+/-}$ as wild−type (WT) and STAT3$^{fl/fl}$;LysM−Cre$^{+/-}$ as knockout (KO) (Figure 1a).

To verify a STAT3 depletion in microglia, STAT3 gene knockout was first confirmed by genotyping (Figure 1b). The absence of microglial STAT3 expression (red, anti−STAT3; green, anti−Iba−1) in the prefrontal cortex of STAT3$^{fl/fl}$;LysM−Cre$^{+/-}$ mice was verified using tissue immunostaining. The profile of immunofluorescence intensity showed that STAT3 was not expressed in microglia (Figure 2). In primary cultured microglial cells (red, anti−Iba−1) obtained from the STAT3−deficient mouse model, the expression of STAT3 (green, anti−STAT3)

was completely depleted in STAT3$^{fl/fl}$;LysM−Cre$^{+/-}$ mice as well as shown in quantitative data (Figure 3a and b; $p < 0.001$). From the immunoblotting analysis, I also confirmed that the STAT3 expression was depleted specifically in microglia, but not in neurons and astrocytes that were isolated from each primary cultured cell (Figure 3c; $p < 0.001$). Additionally, depletion of STAT3 in microglia had no effect on the expression of STAT3 in neurons and on the number of both neurons and microglia in STAT3$^{fl/fl}$;LysM−Cre$^{+/-}$ mice (Figure 4 and Figure 5).

Loss of microglial STAT3 leads to antidepressive−like behavior

To investigate the behavioral correlates of neuron−microglia interactions, I examined mood−related behaviors in the model mice. Interestingly, I observed antidepressive−like behaviors in the tail suspension test, forced swim test, sucrose preference test, and open field test. As animal models of stress−induced depression to validate the stress−resistant behavior, I induced chronic restraint stress for 2 hours a day for 2 weeks. The level of STAT3 phosphorylation were increased in the wild−type, but not in STAT3$^{fl/fl}$;LysM−Cre$^{+/-}$ mice under chronic stress conditions (Figure 6). In the tail suspension and forced swim tests, the immobility time was significantly reduced in STAT3$^{fl/fl}$;LysM−Cre$^{+/-}$ mice both in control and in chronic stress conditions (Figure 7a; genotype × stress interaction: $F_{(1,38)} = 1.443$, $p = 0.237$; genotype effect: $F_{(1,38)} = 24.906$, $p < 0.001$;

stress effect: $F_{(1,38)}$ = 8.469, p = 0.006, and Figure 7b; genotype × stress interaction: $F_{(1,36)}$ = 0.415, p = 0.523; genotype effect: $F_{(1,36)}$ = 23.718, p < 0.001; stress effect: $F_{(1,36)}$ = 38.4, p < 0.001). Under chronic stress conditions, the immobility time of $STAT3^{fl/fl}$;$LysM-Cre^{+/-}$ mice was increased in the forced swim tests, but not in the tail suspension tests (Figure 7b). These results indicate that $STAT3^{fl/fl}$;$LysM-Cre^{+/-}$ mice had intrinsic resistance owing to genetic modification, and showed partial resilience to chronic stress conditions. To ensure consistency among wild-type groups, immobility time was further compared in the tail suspension and forced swim test. The wild-type groups did not differ from each other (Figure 8). Corroborating the generality of these findings, the wild-type mice subject to chronic restraint stress exhibited a significant decrease in sucrose preference. However, the sucrose preference of $STAT3^{fl/fl}$;$LysM-Cre^{+/-}$ mice was higher than wild-type mice under chronic stress conditions (Figure 9a; genotype × stress interaction: $F_{(1,35)}$ = 12.295, p = 0.001; genotype effect: $F_{(1,35)}$ = 15.764, p < 0.001; stress effect: $F_{(1,35)}$ = 15.601, p < 0.001). Both wild-type and $STAT3^{fl/fl}$;$LysM-Cre^{+/-}$ mice showed similar amounts of liquid intake under both control and stressed conditions (Figure 9b; genotype × stress interaction: $F_{(1,35)}$ = 0.573, p = 0.454; genotype effect: $F_{(1,35)}$ = 0.177, p = 0.677; stress effect: $F_{(1,35)}$ = 4.071, p = 0.051). Lastly, I verified reduced locomotor activity of $STAT3^{fl/fl}$;$LysM-Cre^{+/-}$ mice in the open field test

(Figure 10a; $p < 0.05$), but not the exploration time in the center area (Figure 10b). A previous study demonstrated that the stressed mice showed enhanced locomotor activity under the light of modest brightness (Strekalova et al, 2004). My results suggest that antidepressive-like behavior was observed in $STAT3^{fl/fl}$;LysM-$Cre^{+/-}$ mice. Collectively, dysregulation of STAT3 in microglia successfully alleviated depressive and stress-induced behaviors.

In addition, I found no differences in body weight, anxiety-related and motor behaviors of $STAT3^{fl/fl}$;LysM-$Cre^{+/-}$ mice (Figure 11; trial session effect: $F_{(2,30)} = 83.245$, $p < 0.001$; genotype effect: $F_{(1,15)} = 0.008$, $p = 0.931$), demonstrating that deletion of STAT3 in microglia had solely contributed to antidepressive effects. I also tested whether the antidepressive effects could affect other cognitive functions associated with learning and memory, but found neither cognitive impairment nor enhancement in $STAT3^{fl/fl}$;LysM-$Cre^{+/-}$ mice (Figure 12).

Downregulation of microglial STAT3 increases neuronal M-CSF levels in neuron-microglia interactions

To identify key factors affecting antidepressive-like behavior caused by depletion of microglial STAT3, I first examined the cytokine levels in the brain tissue of both wild-type and $STAT3^{fl/fl}$;LysM-$Cre^{+/-}$ mice using a

cytokine array. The data showed that M-CSF was increased solely in STAT3$^{fl/fl}$;LysM-Cre$^{+/-}$ mice (Figure 13; one-way ANOVA: $F_{(1,4)}$ = 9.304, $p < 0.05$). The effect of M-CSF in association with antidepressive-like behavior was highly localized to several brain regions, such as prefrontal cortex, cerebellum, and hippocampus, where M-CSF receptors were primarily expressed (Figure 14a; $p < 0.001$, b; $p < 0.01$, and c; $p < 0.05$). However, I could not detect any change in the levels of canonical cytokines, such as ICAM-1, IL-1β, TNF-α, IL-6 and IL-10 (Figure 14 and Figure 15). These results suggest that M-CSF may be a key factor for regulating antidepressive-like behavior. To determine whether peripheral macrophages had an effect on increasing M-CSF, I applied the same cytokine array to peritoneal macrophages isolated from both wild-type and STAT3$^{fl/fl}$;LysM-Cre$^{+/-}$ mice (Figure 16a and b). sICAM-1 and CCL2 were increased, but CXCL13 was decreased in macrophages of STAT3$^{fl/fl}$;LysM-Cre$^{+/-}$ mice (Figure 16c; CXCL13: $F_{(1,2)}$ = 71.092, $p < 0.05$; sICAM-1: $F_{(1,2)}$ = 22.346, $p < 0.05$; CCL2: $F_{(1,2)}$ = 71.906, $p < 0.05$). These factors were expressed at the similar level in the brain tissue, indicating that M-CSF-mediated antidepressive-like behavior was not associated with peripheral macrophages. In short, the results indicate that M-CSF production regulates antidepressive-like behaviors through neuron-microglia interactions.

To mimic the neuron-microglia interactions of $STAT3^{fl/fl}$;$LysM-Cre^{+/-}$ mouse model, I performed *in vitro* co-culture using transwell inserts with both the neuronal cell line HT22 and the microglia cell line BV2 (Figure 17a). Endogenous STAT3 level was silenced by transfection with specific small interfering RNA for STAT3 (siSTAT3) in BV2 cells with the maintenance of cell viability (Figure 17b and c). Although the mRNA level of STAT3 and ICAM-1 in BV2 cells decreased in the co-culture system, the M-CSF, IL-1β, and TNF-α levels remained unchanged in the cells (Figure 18a; STAT3: $p < 0.001$, ICAM-1: $p < 0.01$). Importantly, the mRNA level of M-CSF increased in HT22 cells co-cultured with STAT3 knocked-down BV2 cells, but no change was observed in the STAT3, ICAM-1, IL-1β and TNF-α mRNA levels (Figure 18b; $p < 0.01$).

Based on the results, I hypothesized that the secretion of M-CSF may occur mainly in neuronal cells. To examine this, I measured the concentration of M-CSF using an ELISA in the co-culture system. The amount of secreted M-CSF was highly increased in the co-culture medium of HT22 cells with STAT3-silenced BV2 cells (Figure 19a; $p < 0.001$); however, that of M-CSF secretion had no difference between the control and STAT3-silenced BV2 cells (Figure 19b). Thus, the data suggest that ablation of STAT3 in microglia is crucial for the increase in

M-CSF production in neuronal cells and that these mechanisms may play a crucial role in neuronal functions, leading to the antidepressive-like behavior in STAT3$^{fl/fl}$;LysM-Cre$^{+/-}$ mice.

In order to examine which factors from microglia could increase the release of M-CSF from neurons, I analyzed the cytokine/chemokine profiles of microglia in the STAT3-deficient mouse model. The results showed that the expression of CCL2 was reduced in primary microglia isolated from STAT3$^{fl/fl}$;LysM-Cre$^{+/-}$ mice as well as in STAT3-silenced BV2 cells from *in vitro* co-culture system (Figure 20). I assumed that CCL2 in microglia contributed to the increase of M-CSF in neurons. However, the following results indicated that CCL2 had no effects on the changes of M-CSF levels in neurons (Figure 21a). Besides, the expression level of CCL2 had no differences between the brains of wild-type and STAT3$^{fl/fl}$;LysM-Cre$^{+/-}$ mice (Figure 21b). These results indicate that CCL2 was not involved in the M-CSF production.

M-CSF upregulates antidepressant signaling pathways and BDNF expression

To identify how the secreted M-CSF triggers the activation of antidepressant signaling pathways, I investigated brain-derived neurotrophic factor (BDNF) levels and signaling cascades of ERK1/2 and

Akt/GSK3β in the STAT3$^{fl/fl}$;LysM−Cre$^{+/-}$ mouse model. I observed that the BDNF expression as well as ERK1/2 and Akt/GSK3β phosphorylation was increased in several brain regions of STAT3$^{fl/fl}$;LysM−Cre$^{+/-}$ mice, including the prefrontal cortex, cerebellum, and hippocampus (Figure 22; all $p < 0.05$). In synaptosomes from the prefrontal cortex of STAT3$^{fl/fl}$;LysM−Cre$^{+/-}$ mice, the phosphorylation of ERK1/2 and Akt/GSK3β was enhanced, along with increased BDNF expression; however, I found no changes in the levels of pre−/post−synaptic proteins, such as synaptophysin, VGLUT1, and PSD95 (Figure 23; all $p < 0.05$). Lastly, I verified the direct effects of M−CSF on ERK1/2 and Akt/GSK3β signaling pathways in a time−dependent manner in synaptosomes from cortical slices of the wild−type mice. M−CSF stimulation gradually increased phosphorylation of ERK1/2 and Akt/GSK3β in synaptic level (Figure 24; ERK1/2 at 30, 60 min, Akt and GSK3β at 30 min: $p < 0.05$, Akt at 15 min and GSK3β at 60 min: $p < 0.01$). The results imply that M−CSF activates antidepressant pathways, along with BDNF production.

I further confirmed the results in *in vitro* co−culture system. The expression of BDNF as well as phosphorylation of ERK1/2 and Akt/GSK3β was increased only in HT22 cells co−cultured with STAT3−silenced BV2 cells (Figure 25; all $p < 0.05$). As expected, BDNF

expression was persistently increased, and both ERK1/2 and Akt/GSK3β remained phosphorylated after M-CSF stimulation for 24 hours in HT22 cells (Figure 26; all $p < 0.05$). Finally, I observed the direct effects of M-CSF within an hour on ERK1/2 and Akt/GSK3β signaling pathways in HT22 cells (Figure 27; ERK1/2 at 60 min, Akt at 30 min, and GSK3β at 15, 30 min: $p < 0.05$, ERK1/2 at 15, 30 min, Akt at 15 min, and GSK3β at 60 min: $p < 0.01$).

However, I found no direct effects of peritoneal macrophages on neuronal cells. ERK1/2 and Akt/GSK3β signaling pathways did not induce any change in HT22 cells with macrophage cell line RAW264.7 medium regardless of whether STAT3 was downregulated or not (Figure 28). I reasoned that the effects of M-CSF stimulation on microglia should be tested since M-CSF was one of the well-known inducers for intracellular signaling in microglia (Imai and Kohsaka, 2002). Data showed that the phosphorylation of ERK1/2 and Akt/GSK3β did not increase in STAT3-silenced BV2 cells (Figure 29). Collectively, these data strongly indicate that M-CSF may be critically involved in antidepressive-like behavior by upregulating BDNF expression through a direct effect on the ERK1/2 and Akt/GSK3β signaling cascades.

As neuronal mechanisms of depression, the increased synaptic transmission could be a potent mechanism from a therapeutic point of view (Duman and Aghajanian, 2012a). Previous study has found that neuronal activation of GSK3β decreases presynaptic glutamate release (Wildburger and Laezza, 2012). In addition, the ERK1/2 intracellular pathway is a major mediator of BDNF which affects presynaptic neurotransmitter release rather than morphological changes of synapses (Hetman *et al*, 1999; Yu and Chen, 2011). In morphological perspectives, Golgi staining showed no differences in the number of dendritic spines between the wild-type and $STAT3^{fl/fl}$;$LysM-Cre^{+/-}$ mice (Figure 30). These results imply that microglia-derived effects could facilitate the release of neurotransmitters on presynaptic synapses. I concluded that elevated M-CSF secretion in neuronal cells caused by interaction with STAT3-deficient microglia presynaptically enhanced glutamatergic neurotransmission.

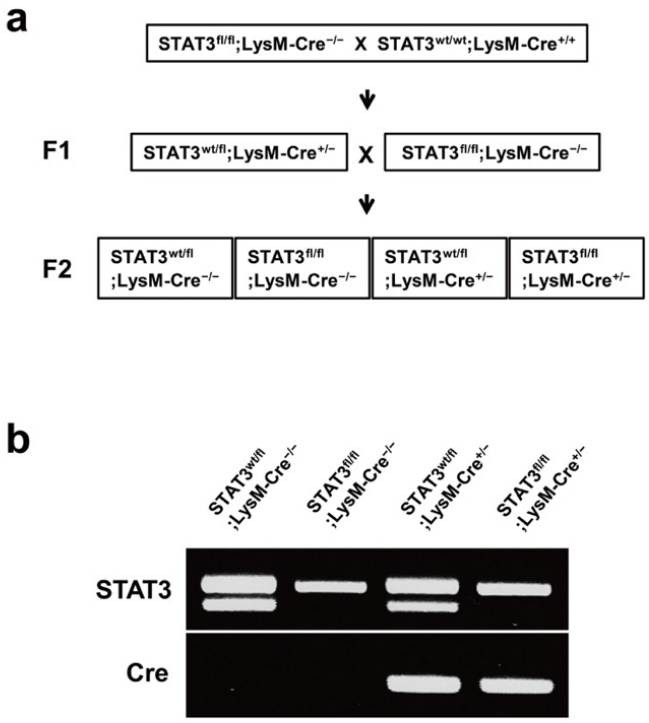

Figure 1. Generation of microglia-specific STAT3 knockout mice by LysM gene targeting

(a) Schematic representation of breeding strategy. The first offspring (F1) were obtained from a $STAT3^{fl/fl}$/LysM-$Cre^{+/+}$ crossing, and $STAT3^{wt/fl}$;LysM-$Cre^{+/-}$ (F1) were further mated with STAT3 floxed mice. The second offspring (F2) were divided into four groups: $STAT3^{wt/fl}$;LysM-$Cre^{-/-}$, $STAT3^{fl/fl}$;LysM-$Cre^{-/-}$, $STAT3^{wt/fl}$;LysM-$Cre^{+/-}$ and $STAT3^{fl/fl}$;LysM-$Cre^{+/-}$. (b) PCR analysis of STAT3 floxed ($STAT3^{fl/fl}$), wild-type ($STAT3^{wt/fl}$) and Cre genes in the second offspring.

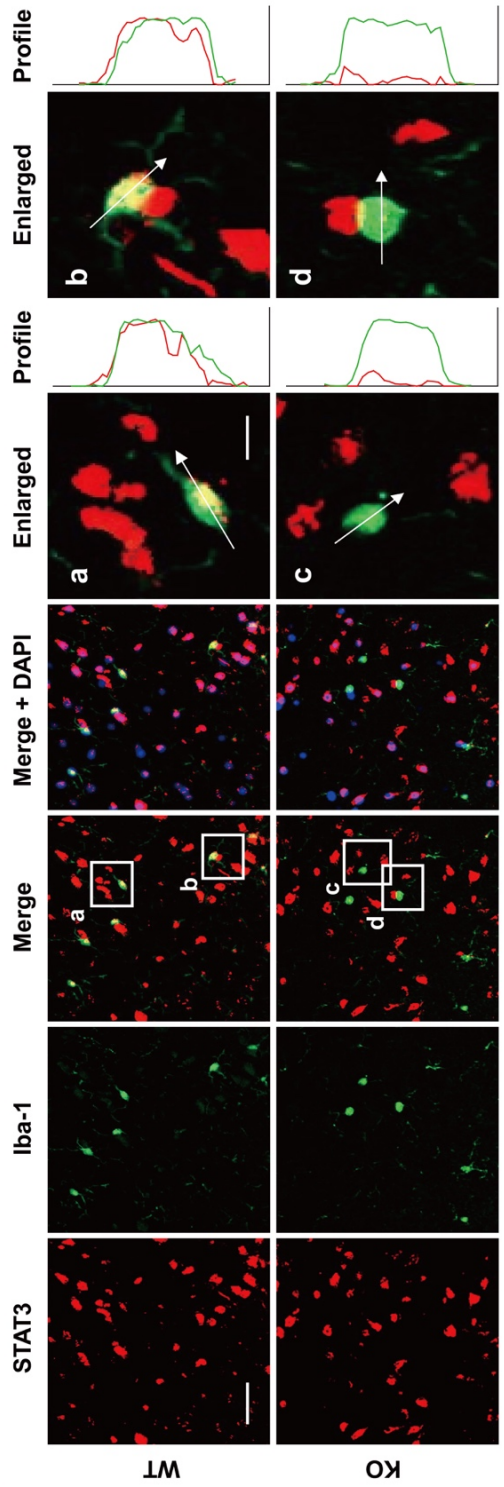
STAT3
Iba-1
Merge
Merge + DAPI
Enlarged
Profile
Enlarged
Profile
WT
KO
a
b
c
d

Figure 2. A microglia-specific deletion of STAT3 in brain tissues of STAT3$^{fl/fl}$;LysM-Cre$^{+/-}$ mice

Immunofluorescence staining for STAT3 (red), Iba-1 (green) and DAPI (blue) was performed in the PFC of the WT and KO mice. Scale bar=40μm. Scale bar of the enlarged image=10μm. The graph shows intensity profiles illustrating STAT3/Iba-1 co-localization measurements.

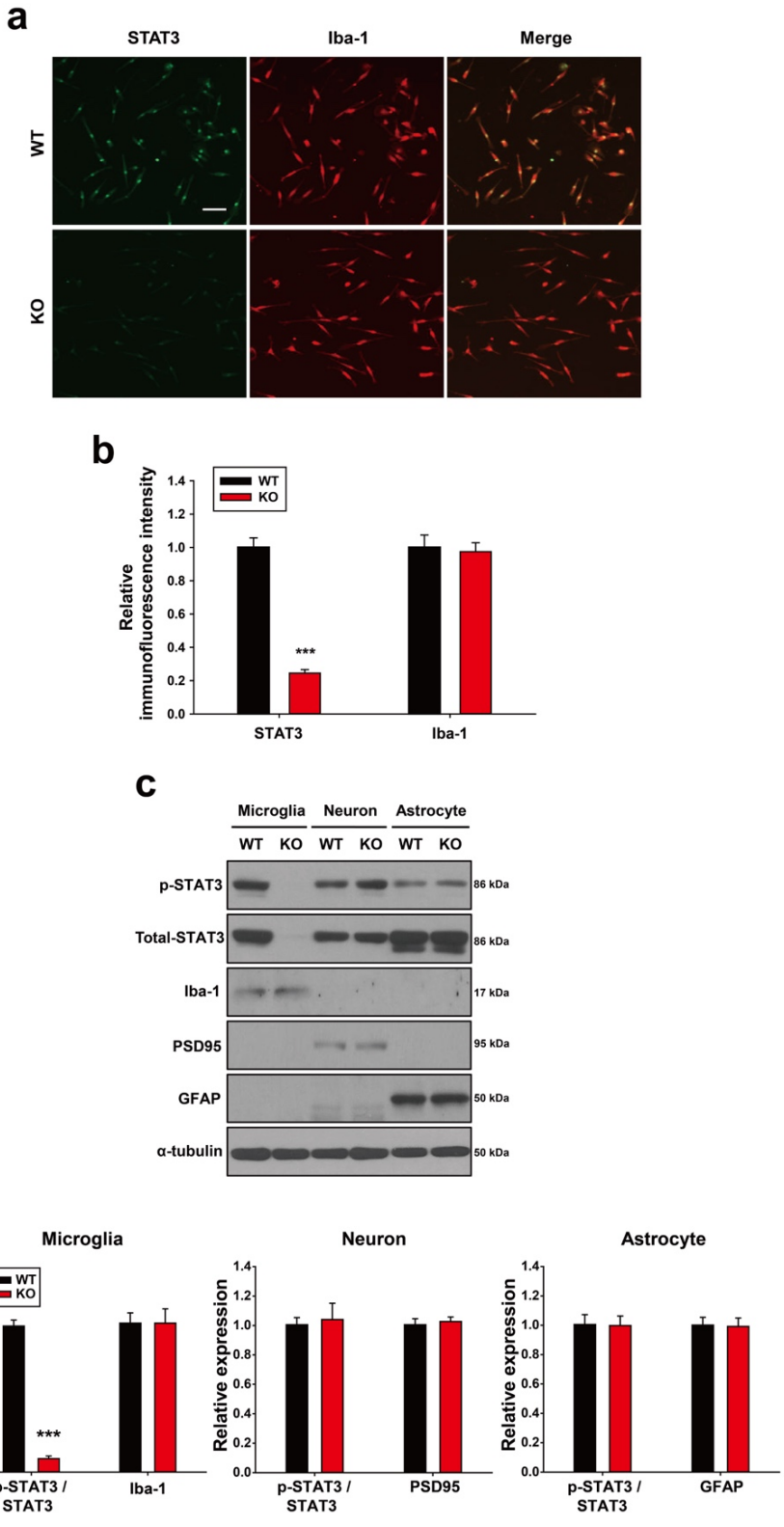
a
STAT3
Iba-1
Merge
WT
KO
b
Relative immunofluorescence intensity
WT
KO
***
STAT3
Iba-1
c
Microglia
Neuron
Astrocyte
WT KO WT KO WT KO
p-STAT3
Total-STAT3
Iba-1
PSD95
GFAP
α-tubulin
86 kDa
86 kDa
17 kDa
95 kDa
50 kDa
50 kDa
Microglia
Neuron
Astrocyte
Relative expression
WT
KO
***
p-STAT3 / STAT3
Iba-1
p-STAT3 / STAT3
PSD95
p-STAT3 / STAT3
GFAP

Figure 3. A specific deletion of STAT3 in primary microglia of STAT3$^{fl/fl}$;LysM−Cre$^{+/-}$ mice

(a) Immunocytochemistry for STAT3 (green) and Iba−1 (red) was performed in the primary microglia cells of the WT and KO mice. Scale bar = 50μm. (b) The relative immunofluorescence intensity was used to represent protein levels of STAT3 and Iba−1 (STAT3; 1 ± 0.058 vs 0.245 ± 0.021, Iba−1; 1 ± 0.075 vs 0.974 ± 0.054 in primary microglia of the WT and KO mice, n = 3 mice / group, respectively). (c) Western blot analysis of STAT3, Iba−1, PSD95 and GFAP in primary microglia, neurons, and astrocytes of the WT and KO mice. Each quantification of Western blot was obtained with relative densitometry and normalized with α−tubulin. Data are means ± SEM, and *p < 0.05, **p < 0.01, ***p < 0.001.

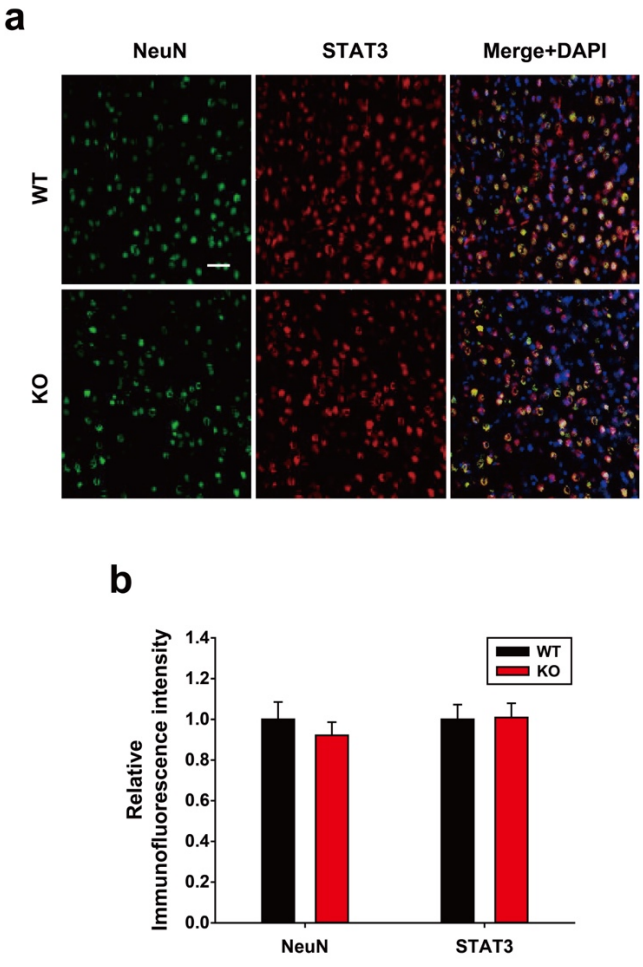
a
NeuN
STAT3
Merge+DAPI
WT
KO
b
Relative Immunofluorescence intensity
1.4
1.2
1.0
0.8
0.6
0.4
0.2
0.0
WT
KO
NeuN
STAT3

Figure 4. Microglia-specific STAT3 KO mice show no difference in STAT3 expression in neurons.

(a) Immunofluorescence staining of NeuN (green), STAT3 (red) and DAPI (blue) was performed in the PFC of the WT and KO mice (Scale bar = 80μm, n = 3 mice/group). (b) The relative immunofluorescence intensity was used to represent protein levels of NeuN and STAT3 (NeuN; 1 ± 0.085 vs 0.921 ± 0.065, STAT3; 1 ± 0.072 vs 1.009 ± 0.07, n = 3 mice/group).

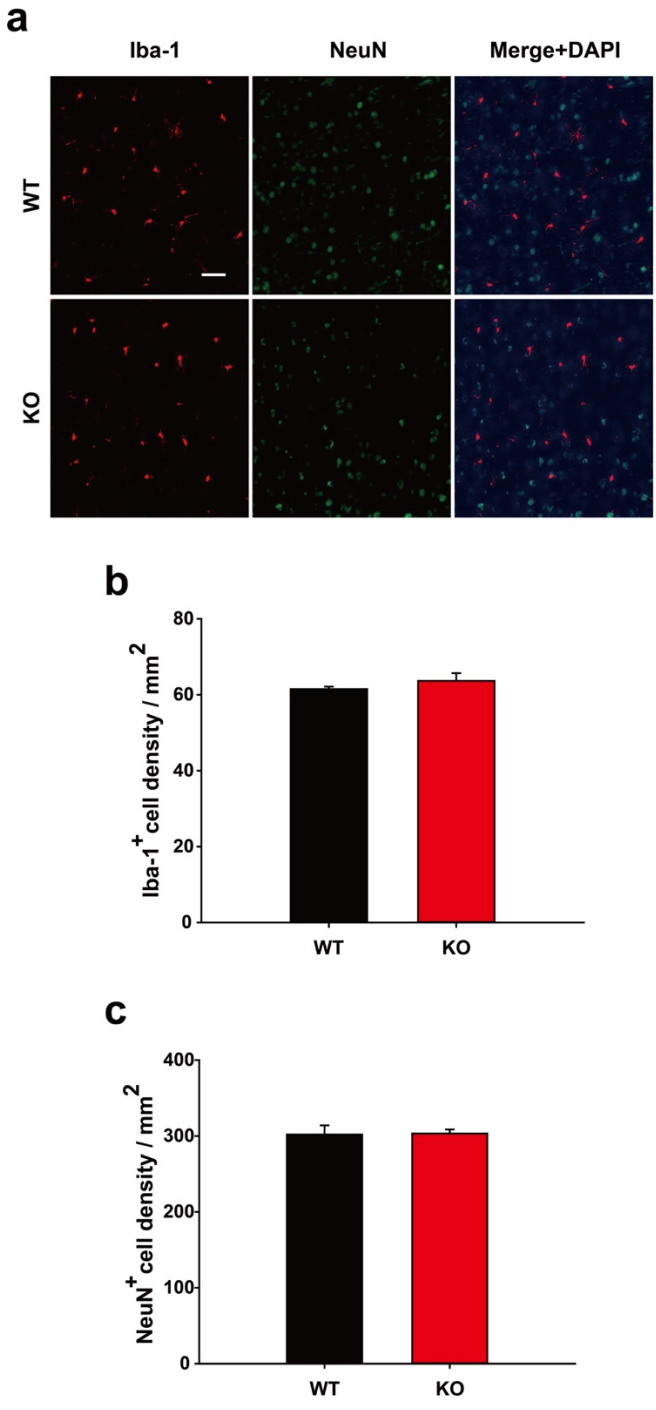
a
Iba-1
NeuN
Merge+DAPI
WT
KO
b
Iba-1+ cell density / mm2
80
60
40
20
0
WT
KO
c
NeuN+ cell density / mm2
400
300
200
100
0
WT
KO

Figure 5. No difference in the number of microglia and neurons between the WT and KO mice

(a) Immunofluorescence staining of Iba−1 (red), NeuN (green) and DAPI (blue) was performed in the PFC of the WT and KO mice (Scale bar = 80μm). (b) Quantification of $Iba{-}1^{+}$ cell density (61.5 ± 0.6 cells/mm^2 vs 63.7 ± 2 cells/mm^2 in the WT and KO mice, n = 5 mice/group). (c) Quantification of $NeuN^{+}$ cell density (302 ± 12 cells/mm^2 vs 303.3 ± 5.3 cells/mm^2 in the WT and KO mice).

Profile
Enlarged
Merge + DAPI
Merge
Iba-1
p-STAT3
a
b
c
d
WT
KO
WT
KO
Control
Stress

Figure 6. Chronic restraint stress enhances STAT3 phosphorylation in microglia of the WT mice.

Immunofluorescence staining for p-STAT3 (red), Iba-1 (green) and DAPI (blue) was performed in the PFC of the WT and KO mice. Scale bar = 40μm. Scale bar of the enlarged image = 10μm. The graph shows intensity profiles illustrating p-STAT3/Iba-1 co-localization measurements.

a

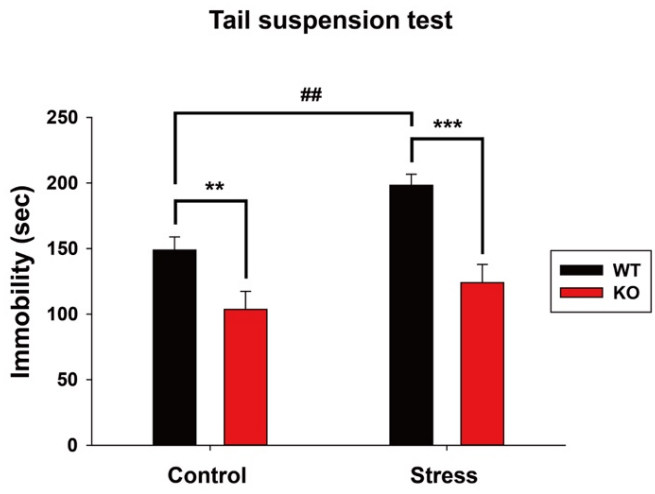
Tail suspension test
##
***
**
250
200
150
100
50
0
Immobility (sec)
WT
KO
Control
Stress

b

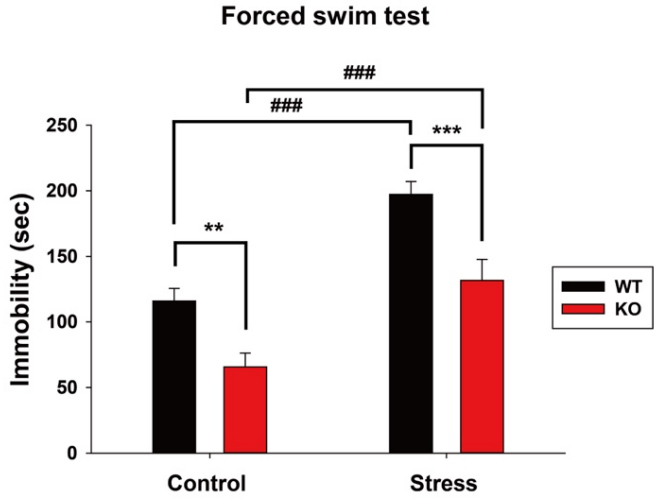
Forced swim test
###
###
***
**
250
200
150
100
50
0
Immobility (sec)
WT
KO
Control
Stress

Figure 7. STAT3$^{fl/fl}$;LysM−Cre$^{+/-}$ mice exhibit antidepressive−like behaviors in the tail suspension and forced swim tests.

(a) Under control or chronic restraint stress conditions, immobility time of the WT and KO mice was assessed by tail suspension test (Control; 148.943 ± 9.943 sec vs 103.537 ± 13.837 sec, n = 12 and 11, Stress; 198.208 ± 8.490 sec vs 124.013 ± 13.878 sec in the WT and KO mice, n = 9 and 10, respectively). (b) Under control or chronic restraint stress conditions, immobility time of the WT and KO mice was assessed by forced swim test (Control; 115.945 ± 9.695 sec vs 65.678 ± 10.593 sec, n = 10 and 11, Stress; 197.328 ± 9.733 sec vs 131.727 ± 16.008 sec in the WT and KO mice, n = 9 and 10, respectively). Data are means ± SEM, *p < 0.05, **p < 0.01, ***p < 0.001 compared with WT; #p < 0.05, ##p < 0.01, ###p < 0.001 compared with control.

a

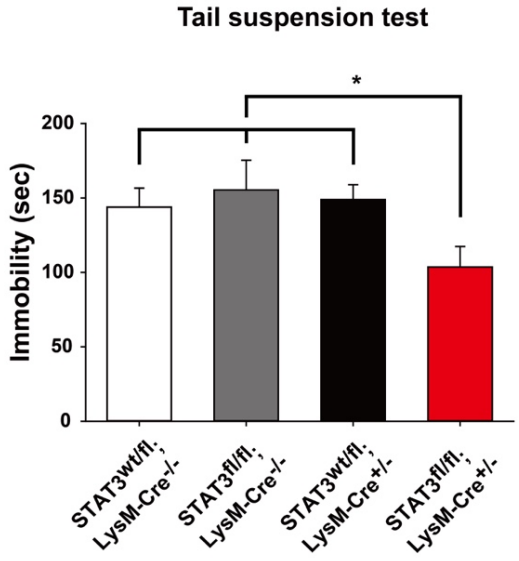
Tail suspension test
*
Immobility (sec)
200
150
100
50
0
STAT3wt/fl; LysM-Cre-/-
STAT3fl/fl; LysM-Cre-/-
STAT3wt/fl; LysM-Cre+/-
STAT3fl/fl; LysM-Cre+/-

b

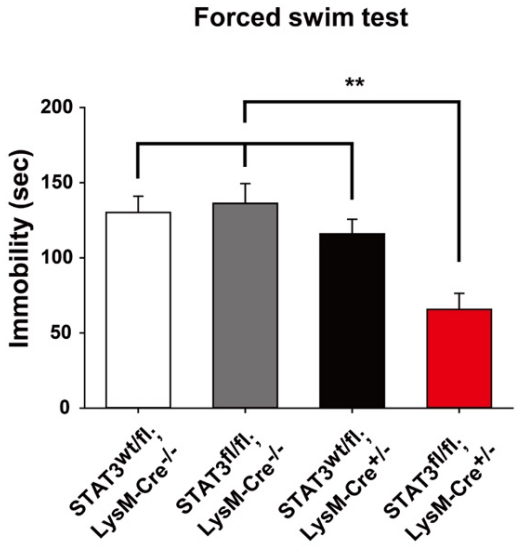
Forced swim test
**
Immobility (sec)
200
150
100
50
0
STAT3wt/fl; LysM-Cre-/-
STAT3fl/fl; LysM-Cre-/-
STAT3wt/fl; LysM-Cre+/-
STAT3fl/fl; LysM-Cre+/-

Figure 8. Wild-type groups are not different in the tail suspension and forced swim tests.

(a) Immobility time of four distinct groups was assessed by tail suspension test ($STAT3^{wt/fl}$;$LysM\text{-}Cre^{-/-}$; 143.87 ± 12.764 sec, $STAT3^{fl/fl}$;$LysM\text{-}Cre^{-/-}$; 155.409 ± 19.913 sec, $STAT3^{wt/fl}$;$LysM\text{-}Cre^{+/-}$; 148.943 ± 9.943 sec, $STAT3^{fl/fl}$;$LysM\text{-}Cre^{+/-}$; 103.537 ± 13.837 sec, n = 10, 12, 12 and 11, respectively) and (b) forced swim test ($STAT3^{wt/fl}$;$LysM\text{-}Cre^{-/-}$; 130.136 ± 10.86 sec, $STAT3^{fl/fl}$;$LysM\text{-}Cre^{-/-}$; 136.256 ± 13.112 sec, $STAT3^{wt/fl}$;$LysM\text{-}Cre^{+/-}$; 115.945 ± 9.695 sec, $STAT3^{fl/fl}$;$LysM\text{-}Cre^{+/-}$; 65.678 ± 19.593 sec, n = 11, 12, 10 and 11, respectively). Data are means ± SEM, and $^{*}p < 0.05$, $^{**}p < 0.01$, $^{***}p < 0.001$.

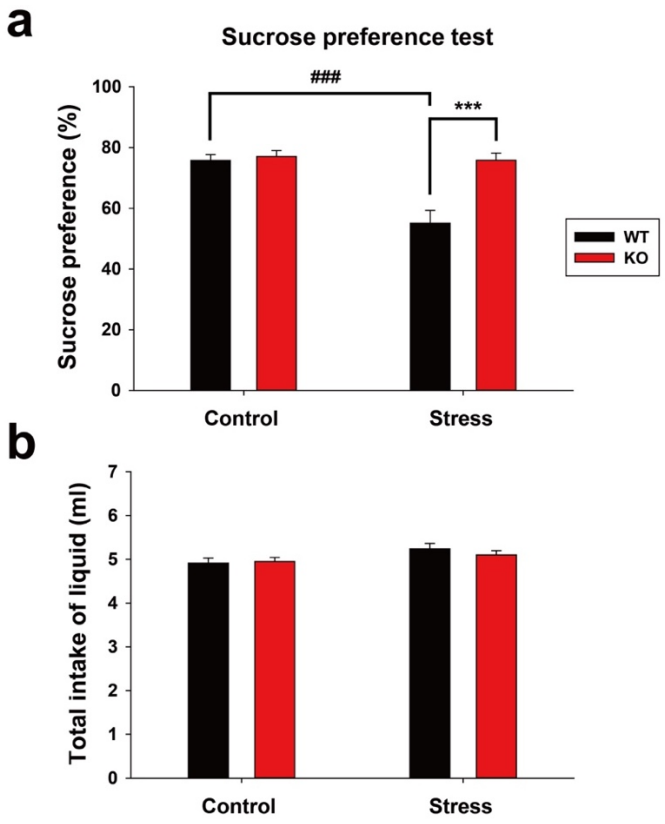
a
Sucrose preference test
###
***
Sucrose preference (%)
100
80
60
40
20
0
WT
KO
Control
Stress
b
Total intake of liquid (ml)
7
6
5
4
3
2
1
0
Control
Stress

Figure 9. STAT3$^{fl/fl}$;LysM−Cre$^{+/-}$ mice show antidepressive−like behaviors in the sucrose preference.

(a) Preference for sucrose under control or chronic restraint stress conditions (Control; 75.776 ± 1.914 % vs 77.061 ± 1.943%, Stress; 55.13 ± 4.146 % vs 75.833 ± 2.341 % in the WT and KO mice, n = 10 and 9, respectively). (b) Total liquid intake under control or chronic restraint stress conditions (Control; 4.91 ± 0.119 ml vs 4.95 ± 0.092 ml, Stress; 5.24 ± 0.121 ml vs 5.1 ± 0.097 ml in the WT and KO mice, n = 10 and 9, respectively). Data are means ± SEM, *p < 0.05, **p < 0.01, ***p < 0.001 compared with WT; #p < 0.05, ##p < 0.01, ###p < 0.001 compared with control.

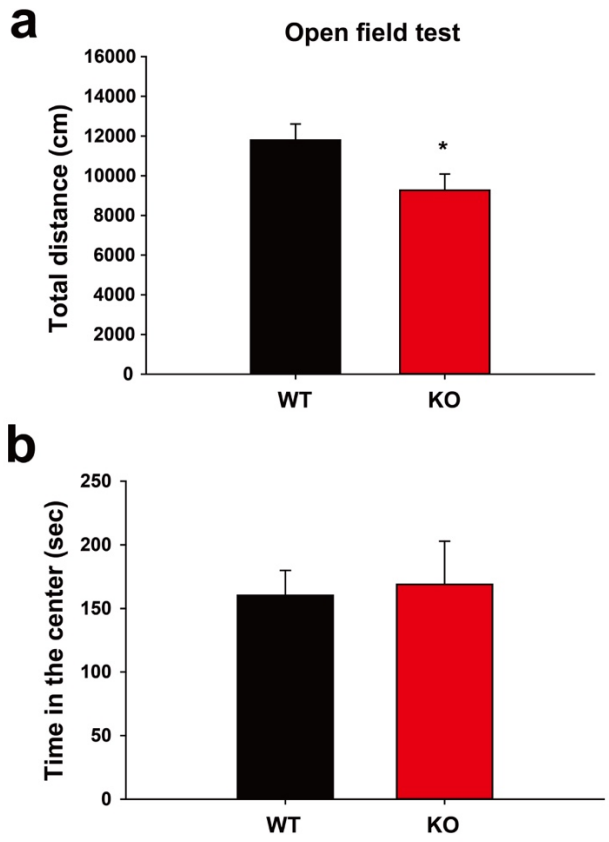

Figure 10. STAT3$^{fl/fl}$;LysM−Cre$^{+/-}$ mice does not show anxiety in the open field tests, but exhibits antidepressive−like behaviors.

(a) Total distance (11794.746 ± 811.651 cm vs 9267.810 ± 819.674 cm in the WT and KO mice) and (b) time spent in the center of the open field (160.3 ± 19.6 sec vs 168.9 ± 34 sec in the WT and KO mice, n = 8 and 9, respectively). Data are means ± SEM, *p < 0.05, **p < 0.01, ***p < 0.001.

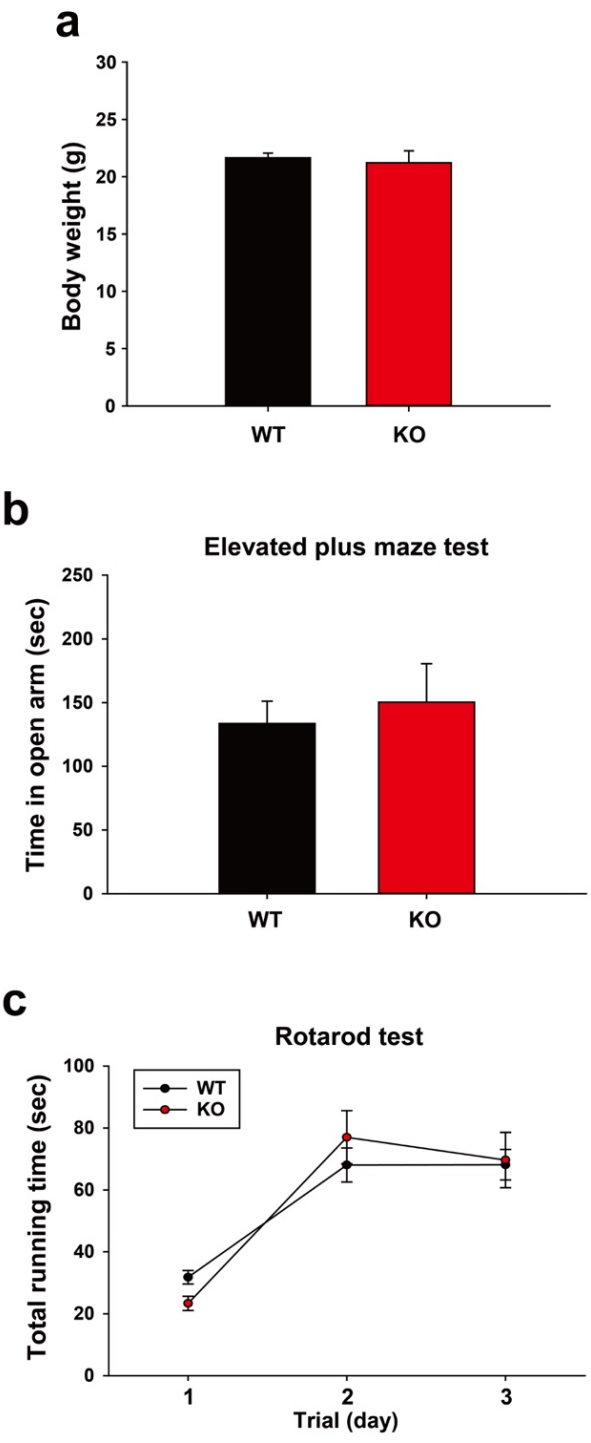
a
Body weight (g)
30
25
20
15
10
5
0
WT
KO
b
Elevated plus maze test
Time in open arm (sec)
250
200
150
100
50
0
WT
KO
c
Rotarod test
Total running time (sec)
100
80
60
40
20
0
WT
KO
1
2
3
Trial (day)

Figure 11. No difference in body weight, anxiety, and locomotor function between the WT and KO mice

(a) Body weight of male mice aged 8 weeks (21.7 ± 0.4 g vs 21.2 ± 1 g in the WT and KO mice, n = 10 and 7, respectively). (b) Time spent in the open arms of plus arms (133.6 ± 17.5 sec vs 150.4 ± 30.2 sec in the WT and KO mice, n = 8 and 9, respectively). (c) Total running time on the rotating drum (n = 8 and 9, respectively).

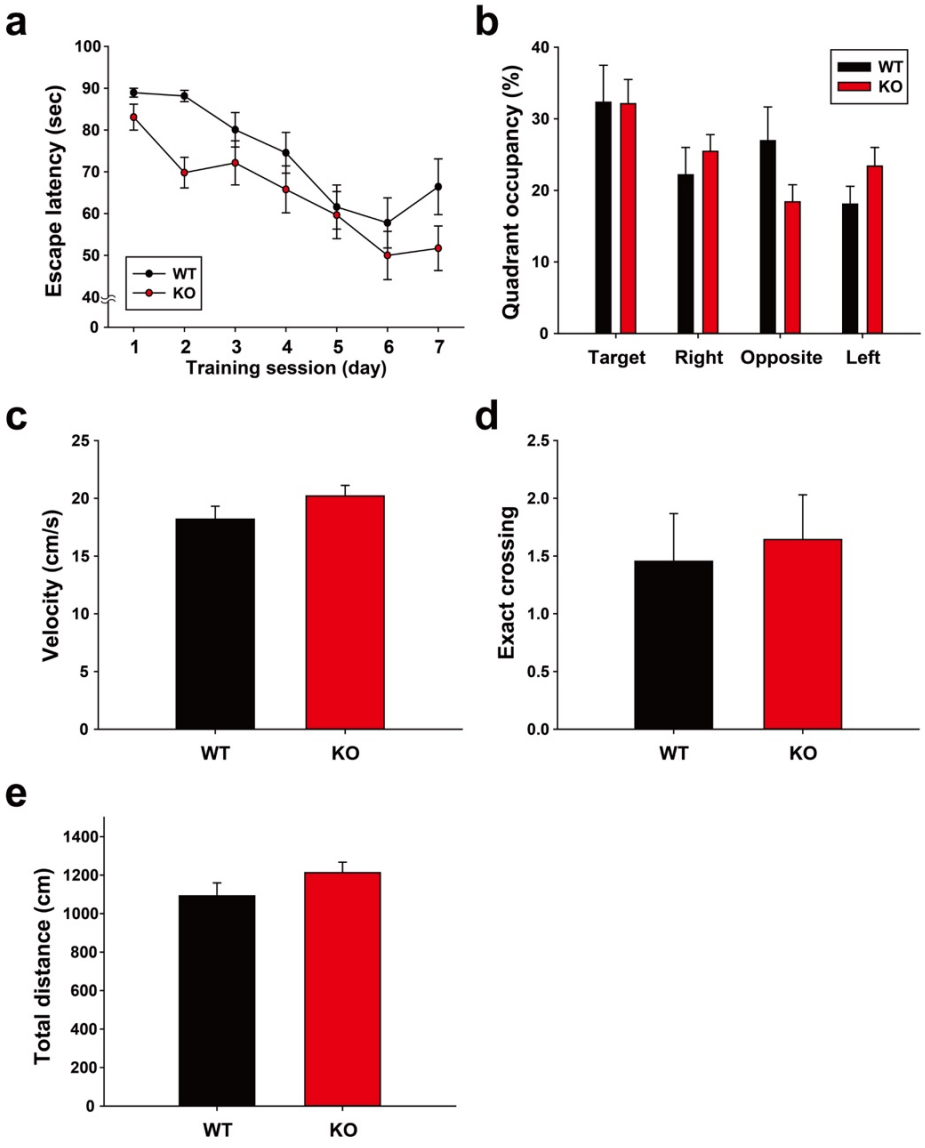
a
Escape latency (sec)
Training session (day)
WT
KO
b
Quadrant occupancy (%)
Target
Right
Opposite
Left
WT
KO
c
Velocity (cm/s)
WT
KO
d
Exact crossing
WT
KO
e
Total distance (cm)
WT
KO

Figure 12. No difference in cognitive function between the WT and KO mice

(a) Morris water maze test was performed for 7 consecutive days, and the escape latency was measured (n = 11 and 14). The repeated two-way ANOVA test indicated a significant main effect of training sessions ($F(6,192) = 15.679$; $p < 0.001$) but a main effect of genotype ($F(1,32) = 4.095$; $p = 0.051$). (b) The quadrant occupancy, (c) the velocity (18.2 ± 1.1 cm/s vs 20.2 ± 0.9 cm/s in the WT and KO mice, respectively), (d) the number of crossing (1.46 ± 0.41 vs 1.64 ± 0.39 in the WT and KO mice, respectively), and (e) the total traveled distance (1092.1 ± 67.9 cm vs 1212.4 ± 54.8 cm in the WT and KO mice, respectively) of the probe test were measured 24 hours after the final trial.

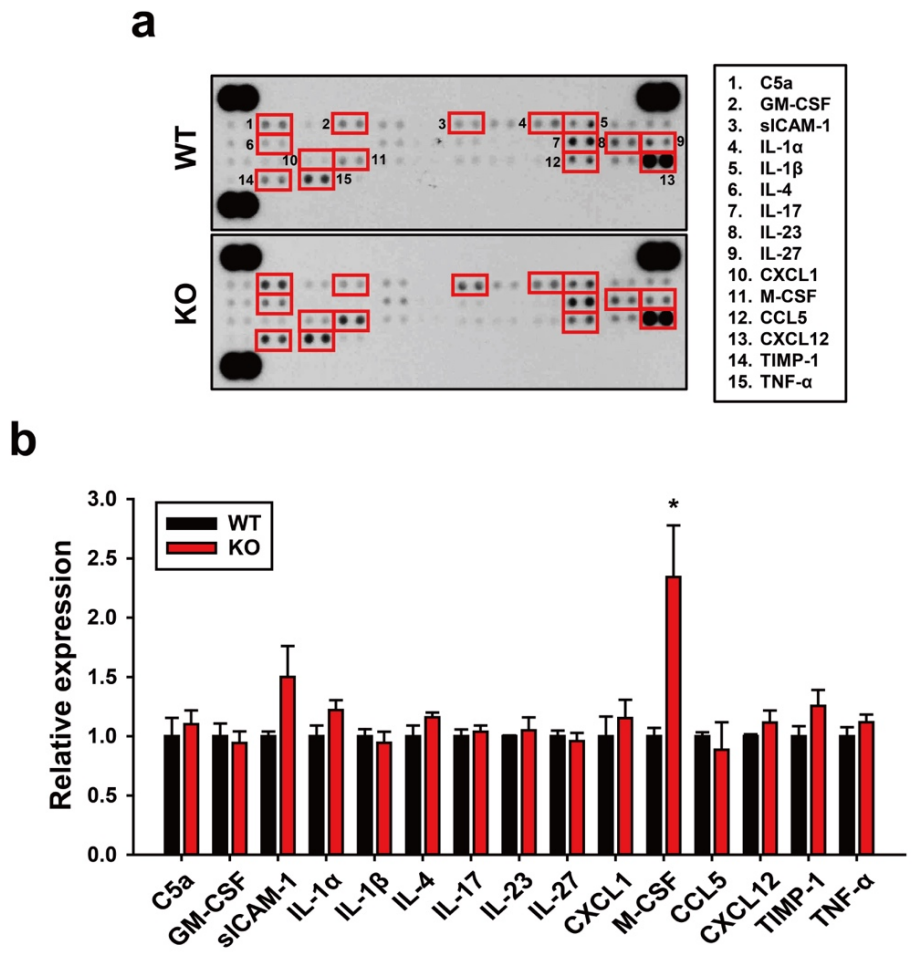

Figure 13. Detection of multiple cytokines in the whole brain tissues of the WT and KO mice

(a) Expression of cytokines and chemokines in the whole brain tissues of the WT and KO mice using cytokine arrays. (b) The bar graph was calculated for each cytokine with mean pixel density. Representative data from three independent experiments are shown.

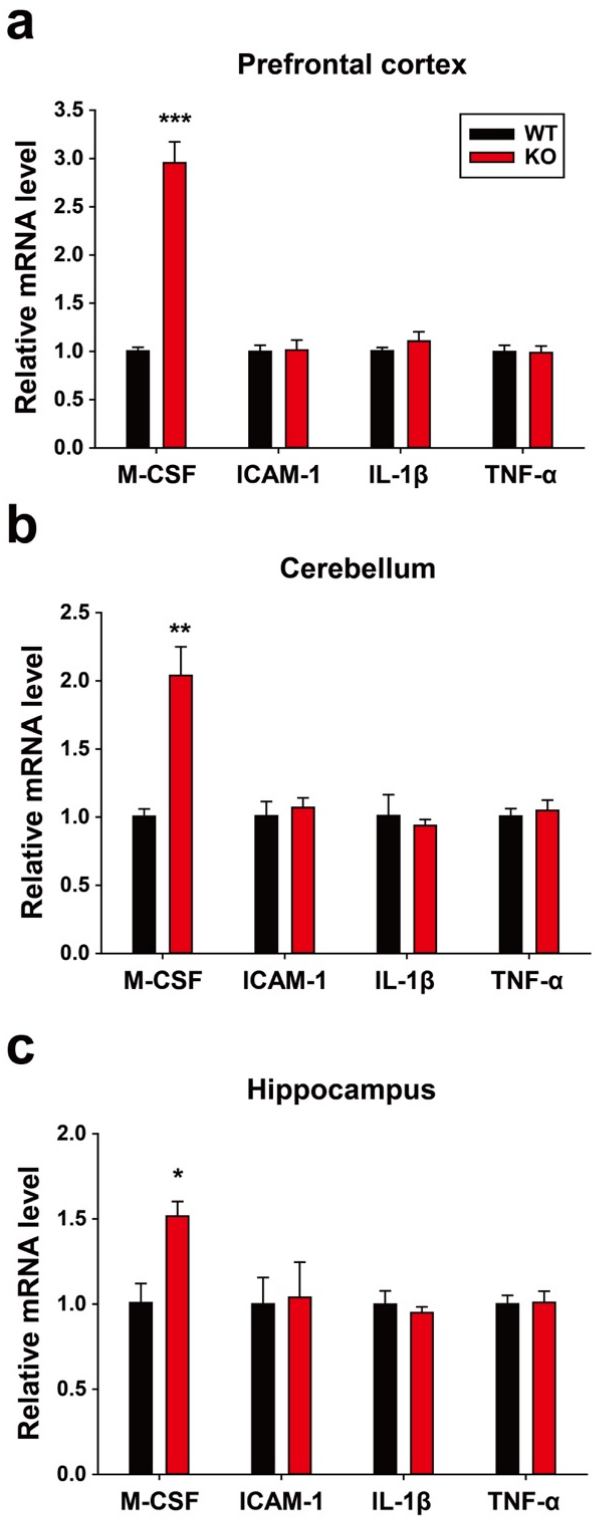
a
Prefrontal cortex
Relative mRNA level
3.5
3.0
2.5
2.0
1.5
1.0
0.5
0.0
***
WT
KO
M-CSF
ICAM-1
IL-1β
TNF-α
b
Cerebellum
Relative mRNA level
2.5
2.0
1.5
1.0
0.5
0.0
**
M-CSF
ICAM-1
IL-1β
TNF-α
c
Hippocampus
Relative mRNA level
2.0
1.5
1.0
0.5
0.0
*
M-CSF
ICAM-1
IL-1β
TNF-α

Figure 14. mRNA levels of canonical cytokines in various brain regions

(a) Relative mRNA levels of M-CSF, ICAM-1, IL-1β and TNF-α in the prefrontal cortex, (b) cerebellum and (c) hippocampus. Representative data from three independent experiments are shown.

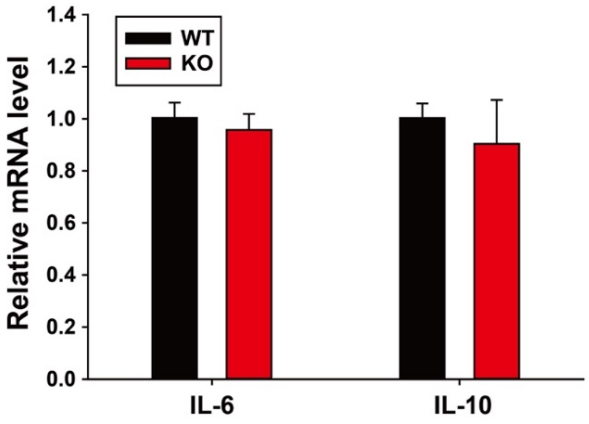

Figure 15. mRNA levels of STAT3 target genes in the whole brain of the WT and KO mice

Relative mRNA levels of IL-6 and IL-10 were quantified by qRT-PCR (IL-6; 1.003 ± 0.058 vs 0.957 ± 0.061, IL-10; 1.003 ± 0.056 vs 0.903 ± 0.169 in the WT and KO mice, n = 3/group, respectively).

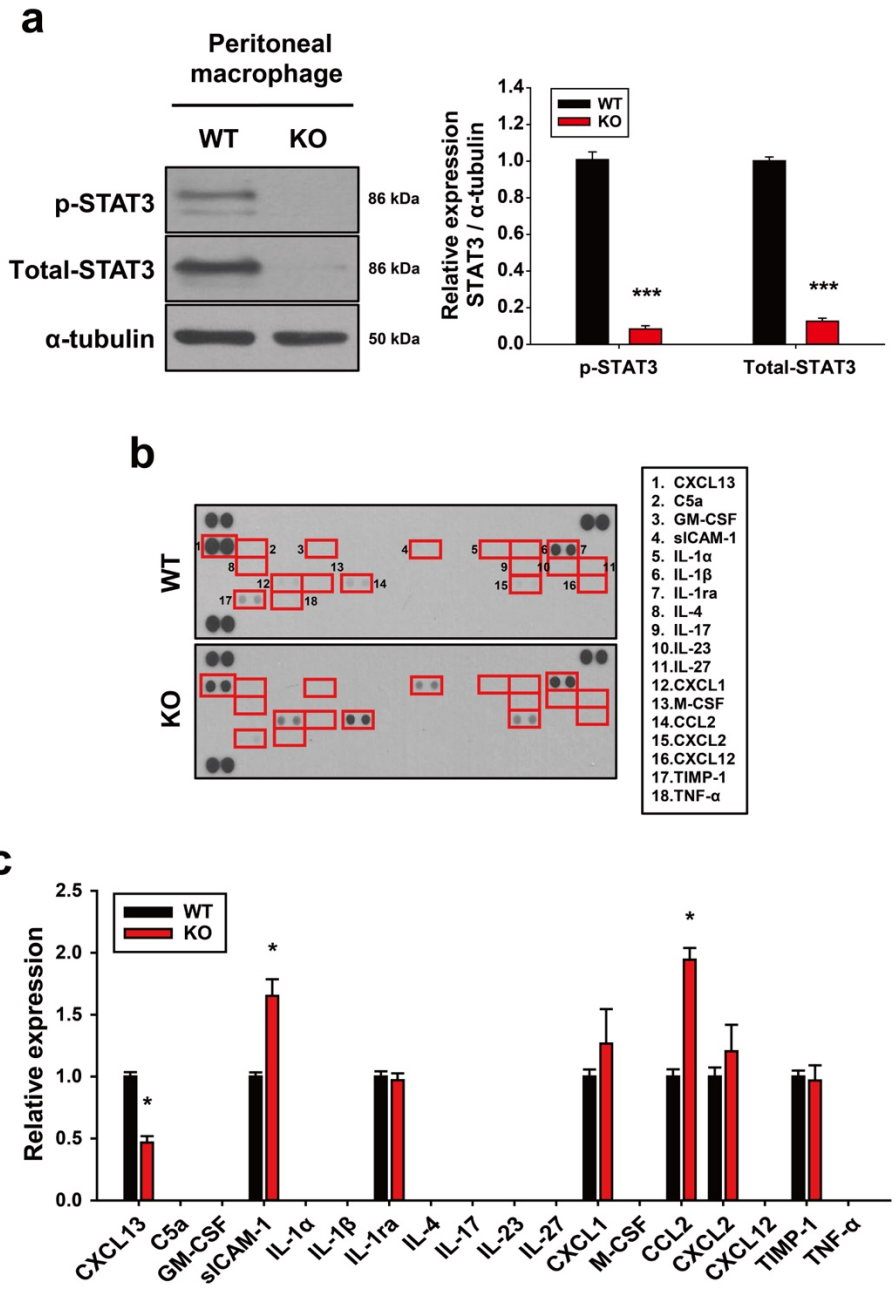
a
Peritoneal macrophage
WT
KO
p-STAT3
Total-STAT3
α-tubulin
86 kDa
86 kDa
50 kDa
Relative expression STAT3 / α-tubulin
WT
KO
***
***
p-STAT3
Total-STAT3
b
WT
KO
1. CXCL13
2. C5a
3. GM-CSF
4. sICAM-1
5. IL-1α
6. IL-1β
7. IL-1ra
8. IL-4
9. IL-17
10.IL-23
11.IL-27
12.CXCL1
13.M-CSF
14.CCL2
15.CXCL2
16.CXCL12
17.TIMP-1
18.TNF-α
c
Relative expression
WT
KO
CXCL13
C5a
GM-CSF
sICAM-1
IL-1α
IL-1β
IL-1ra
IL-4
IL-17
IL-23
IL-27
CXCL1
M-CSF
CCL2
CXCL2
CXCL12
TIMP-1
TNF-α

Figure 16. Detection of multiple cytokines in peripheral macrophages of the WT and KO mice

(a) Western blot analysis of STAT3 in peritoneal macrophages isolated from the WT and KO mice. (b) Expression of cytokines and chemokines in the peritoneal macrophages of the WT and KO mice using cytokine arrays. (c) The bar graph was calculated for each cytokine with men pixel density. Each quantification of Western blot was obtained with relative densitometry and normalized with α-tubulin. Data are means ± SEM, and *$p < 0.05$, **$p < 0.01$, ***$p < 0.001$. Representative data from three independent experiments are shown.

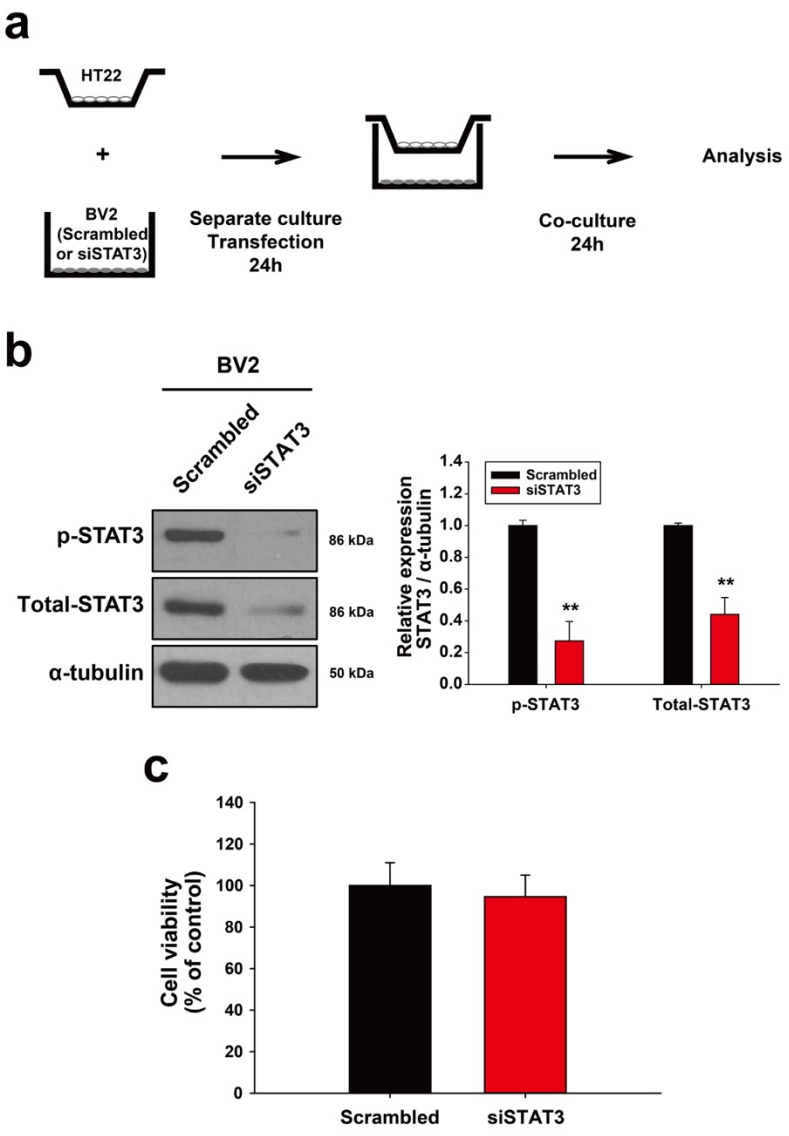
a
HT22
+
BV2
(Scrambled
or siSTAT3)
Separate culture
Transfection
24h
Co-culture
24h
Analysis
b
BV2
Scrambled
siSTAT3
p-STAT3
Total-STAT3
α-tubulin
86 kDa
86 kDa
50 kDa
Relative expression
STAT3 / α-tubulin
Scrambled
siSTAT3
1.4
1.2
1.0
0.8
0.6
0.4
0.2
0.0
**
**
p-STAT3
Total-STAT3
c
Cell viability
(% of control)
140
120
100
80
60
40
20
0
Scrambled
siSTAT3

Figure 17. Interactions between neurons and microglia using *in vitro* co-culture system

(a) Schematic representation of the co-culture system between BV2 and HT22 cells. (b) Western blot analysis of STAT3 and (c) cell viability (100 ± 11 % vs 94.636 ± 10.4 % in scrambled and siSTAT3, n = 3/group, respectively) in BV2 cells after scrambled or STAT3 siRNAs transfection. Each quantification of Western blot was obtained with relative densitometry and normalized with α-tubulin. Data are means ± SEM, and *$p < 0.05$, **$p < 0.01$, ***$p < 0.001$. Representative data from three independent experiments are shown.

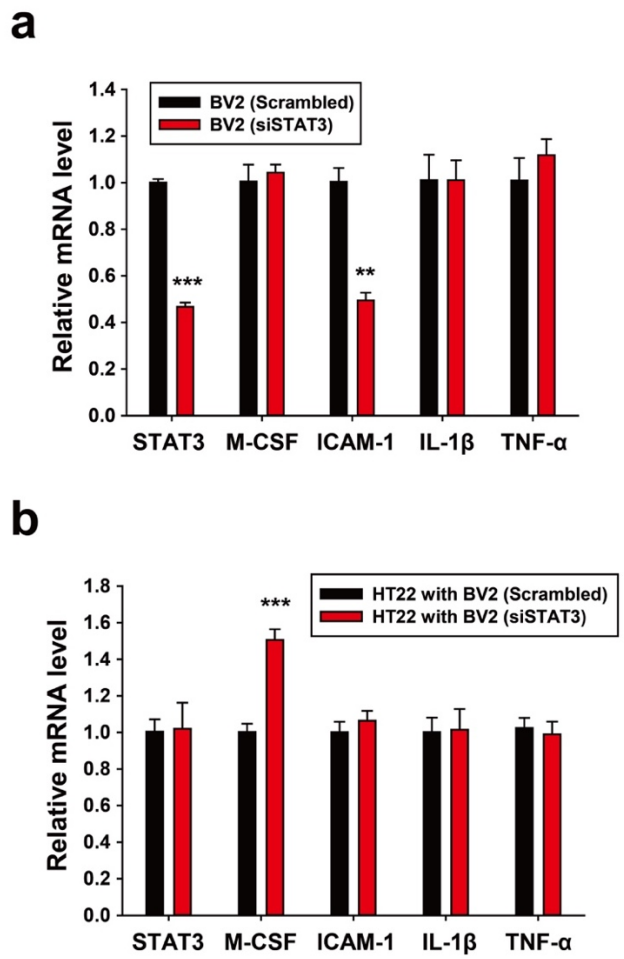

Figure 18. Effects of STAT3-deficient microglia on neuronal M-CSF production in neuron-microglia interactions

(a) Relative mRNA levels of STAT3, M-CSF, ICAM-1, IL-1β and TNF-α in BV2 cells and (b) HT22 cells from the co-culture system was quantified by qRT-PCR. Each quantification of Western blot was obtained with relative densitometry and normalized with α-tubulin. Data are means ± SEM, and *p < 0.05, **p < 0.01, ***p < 0.001. Representative data from three independent experiments are shown.

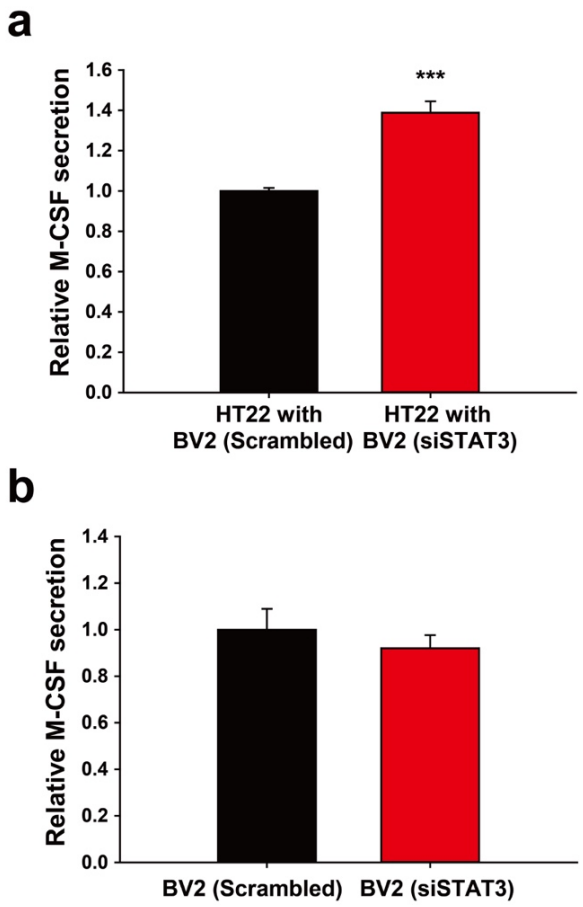

Figure 19. Increased M-CSF secretion in neurons by STAT3-deficient microglia

(a) Concentration of M-CSF from the co-cultured medium (217 ± 3.4pg/ml vs 300 ± 9pg/ml, n = 8/group, respectively) and (b) the BV2-cultured medium (29.2 ± 2.6pg/ml vs 26.7 ± 2.2pg/ml, n = 3/group, respectively) were determined by ELISA. Data are means ± SEM, and *$p < 0.05$, **$p < 0.01$, ***$p < 0.001$.

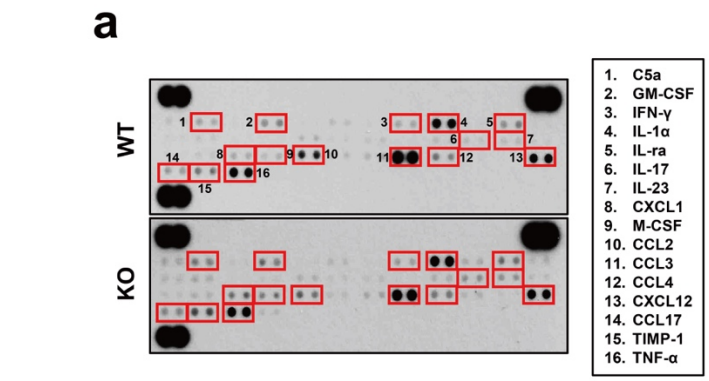
a
WT
KO
1
2
3
4
5
6
7
8
9
10
11
12
13
14
15
16
1. C5a
2. GM-CSF
3. IFN-γ
4. IL-1α
5. IL-ra
6. IL-17
7. IL-23
8. CXCL1
9. M-CSF
10. CCL2
11. CCL3
12. CCL4
13. CXCL12
14. CCL17
15. TIMP-1
16. TNF-α

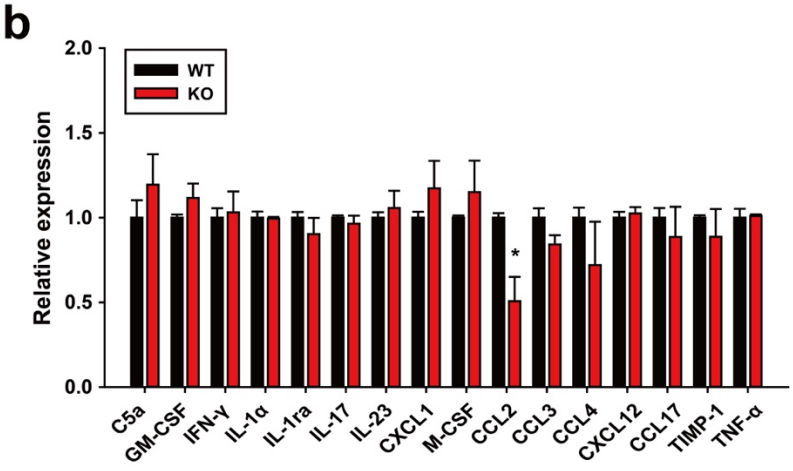
b
Relative expression
2.0
1.5
1.0
0.5
0.0
WT
KO
*
C5a
GM-CSF
IFN-γ
IL-1α
IL-1ra
IL-17
IL-23
CXCL1
M-CSF
CCL2
CCL3
CCL4
CXCL12
CCL17
TIMP-1
TNF-α

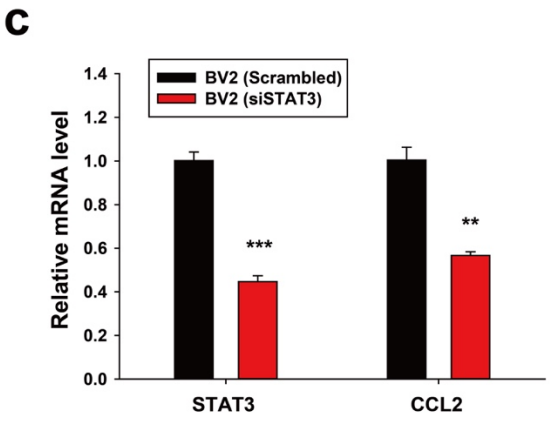
c
Relative mRNA level
1.4
1.2
1.0
0.8
0.6
0.4
0.2
0.0
BV2 (Scrambled)
BV2 (siSTAT3)
***
**
STAT3
CCL2

Figure 20. Detection of multiple cytokines in the primary microglia of the WT and KO mice

(a) Expression of cytokines and chemokines in the cultured medium of primary microglia isolated from the WT and KO mice was determined using cytokine arrays. (b) Bar graph was calculated for each cytokine with mean pixel density. (c) Relative mRNA level of BV2 cells-transfected with either scrambled or siSTAT3 was quantified by qRT-PCR with primers for STAT3 and CCL2 (STAT3; 1.002 ± 0.04 vs 0.447 ± 0.027, CCL2; 1.004 ± 0.06 vs 0.567 ± 0.017 in scrambled and siSTAT3, n = 3/group, respectively). Data are means ± SEM, and *p < 0.05, **p < 0.01, ***p < 0.001. Representative data from three independent experiments are shown.

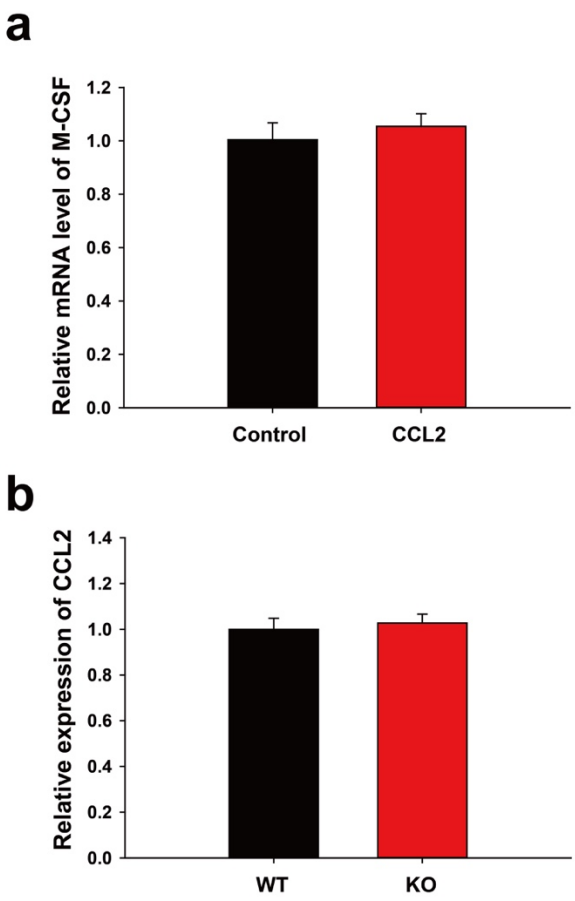

Figure 21. CCL2 does not influence M-CSF expression in neurons.

(a) Relative mRNA level of M-CSF in HT22 cells after CCL2 (100ng/ml) stimulation for 24 hours (1.004 ± 0.064 vs 1.054 ± 0.047 in the control and CCL2 groups, n = 3/group, respectively). (b) Expression of CCL2 in the whole brain of the WT and KO mice using cytokine arrays (1.005 ± 0.061 vs 1.027 ± 0.055 in the WT and KO mice, n = 3/group, respectively). Representative data from three independent experiments are shown.

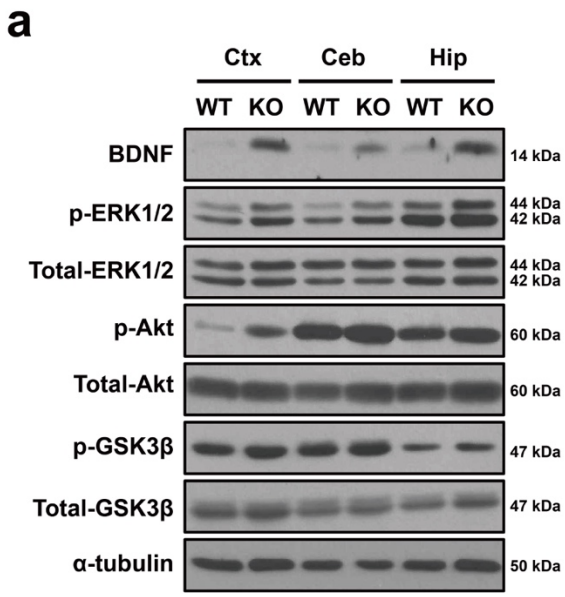
a
Ctx
Ceb
Hip
WT KO WT KO WT KO
BDNF
14 kDa
p-ERK1/2
44 kDa
42 kDa
Total-ERK1/2
44 kDa
42 kDa
p-Akt
60 kDa
Total-Akt
60 kDa
p-GSK3β
47 kDa
Total-GSK3β
47 kDa
α-tubulin
50 kDa

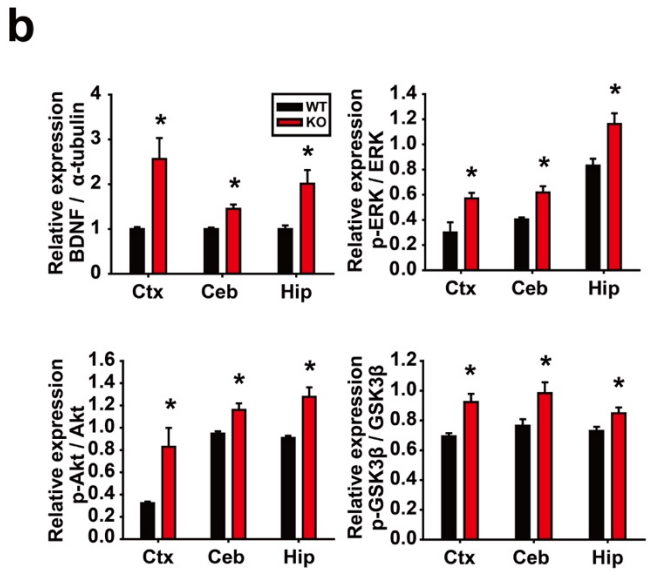
b
Relative expression BDNF / α-tubulin
WT
KO
Ctx
Ceb
Hip
Relative expression p-ERK / ERK
Relative expression p-Akt / Akt
Relative expression p-GSK3β / GSK3β

Figure 22. Antidepressant signaling pathways are significantly activated in the brain of STAT3$^{fl/fl}$;LysM−Cre$^{+/-}$ mice.

(a) Western blot analysis of BDNF, ERK1/2, Akt and GSK3β in the prefrontal cortex (ctx), cerebellum (ceb) and hippocampus (hip) of the WT and KO mice. (b) Quantification of Western blot was obtained with relative densitometry and normalized with α−tubulin. Data are means ± SEM, and *p < 0.05, **p < 0.01, ***p < 0.001. Representative data from three independent experiments are shown.

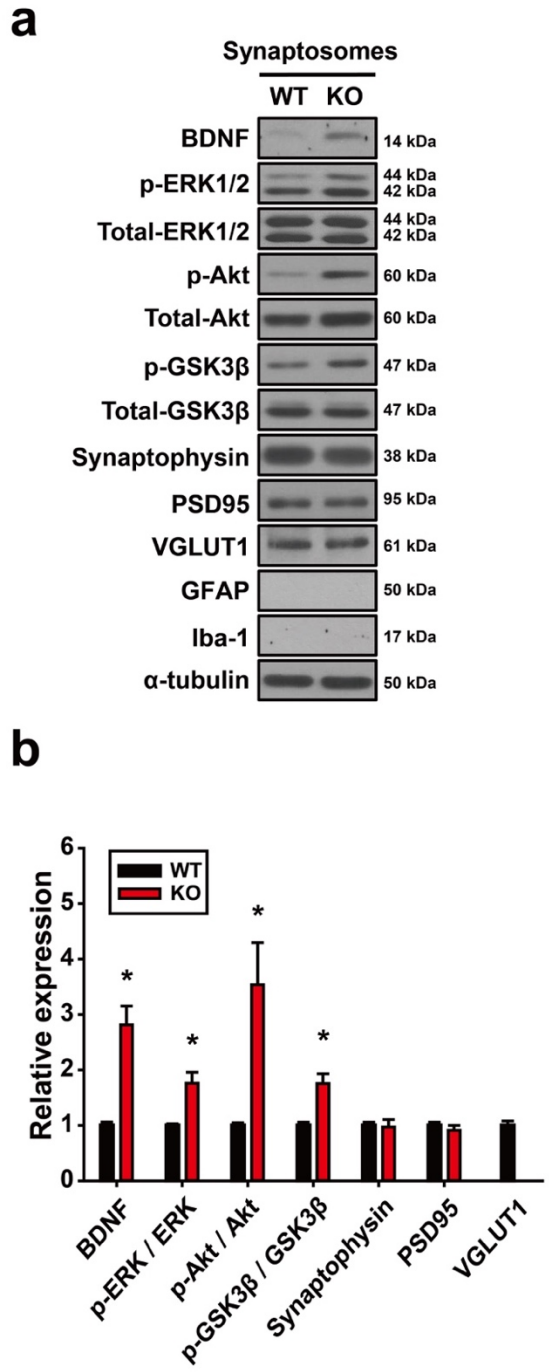
a
Synaptosomes
WT KO
BDNF
p-ERK1/2
Total-ERK1/2
p-Akt
Total-Akt
p-GSK3β
Total-GSK3β
Synaptophysin
PSD95
VGLUT1
GFAP
Iba-1
α-tubulin
14 kDa
44 kDa
42 kDa
44 kDa
42 kDa
60 kDa
60 kDa
47 kDa
47 kDa
38 kDa
95 kDa
61 kDa
50 kDa
17 kDa
50 kDa
b
Relative expression
WT
KO
0
1
2
3
4
5
6
*
*
*
*
BDNF
p-ERK / ERK
p-Akt / Akt
p-GSK3β / GSK3β
Synaptophysin
PSD95
VGLUT1

Figure 23. Activated antidepressant signaling pathways are observed in the synaptosomes from STAT3$^{fl/fl}$;LysM−Cre$^{+/-}$ mice

(a) Western blot analysis of BDNF, ERK1/2, Akt, GSK3β, synaptophysin, PSD95, VGLUT1, GFAP and Iba−1 in the synaptosomes isolated from the PFC of the WT and KO mice. (b) Quantification of Western blot was obtained with relative densitometry and normalized with α−tubulin. Data are means ± SEM, and *p < 0.05, **p < 0.01, ***p < 0.001. Representative data from three independent experiments are shown.

a

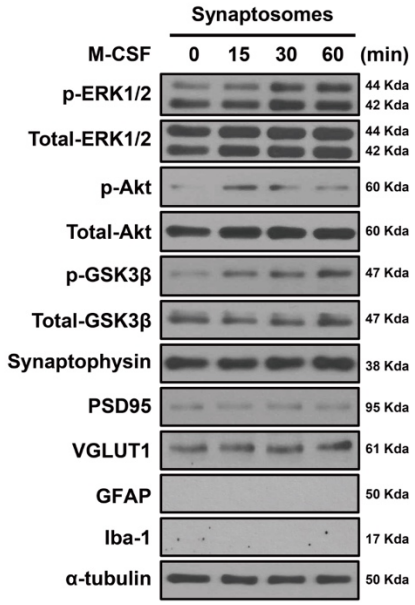
Synaptosomes
M-CSF 0 15 30 60 (min)
p-ERK1/2
44 Kda
42 Kda
Total-ERK1/2
44 Kda
42 Kda
p-Akt
60 Kda
Total-Akt
60 Kda
p-GSK3β
47 Kda
Total-GSK3β
47 Kda
Synaptophysin
38 Kda
PSD95
95 Kda
VGLUT1
61 Kda
GFAP
50 Kda
Iba-1
17 Kda
α-tubulin
50 Kda

b

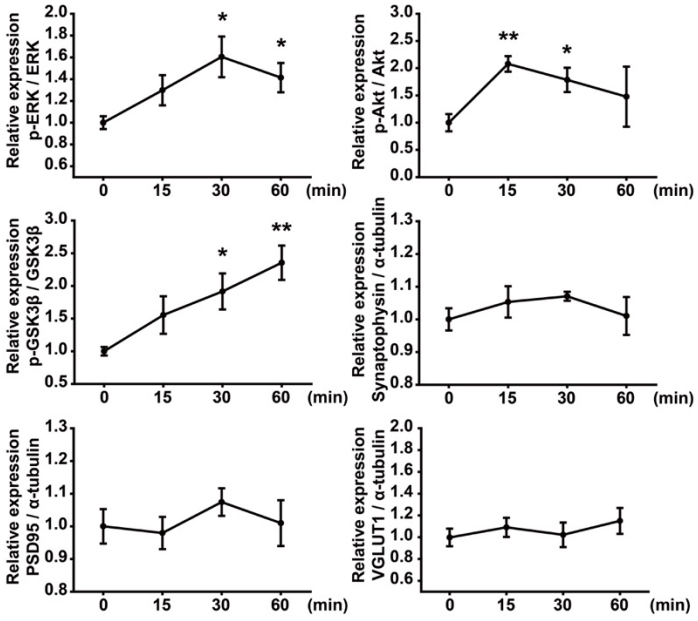
Relative expression p-ERK / ERK
Relative expression p-Akt / Akt
Relative expression p-GSK3β / GSK3β
Relative expression Synaptophysin / α-tubulin
Relative expression PSD95 / α-tubulin
Relative expression VGLUT1 / α-tubulin
0 15 30 60 (min)

Figure 24. M-CSF enhances the activation of antidepressant signaling pathways in the brain of STAT3$^{fl/fl}$;LysM-Cre$^{+/-}$ mice.

(a) Western blot analysis of ERK1/2, Akt, GSK3β, synaptophysin, PSD95, VGLUT1, GFAP and Iba-1 in the synaptosomes isolated from PFC slices of the WT mice after a time-dependent M-CSF stimulation (10 nM). (b) Quantification of Western blot was obtained with relative densitometry and normalized with α-tubulin. Data are means ± SEM, and *p < 0.05, **p < 0.01, ***p < 0.001. Representative data from three independent experiments are shown.

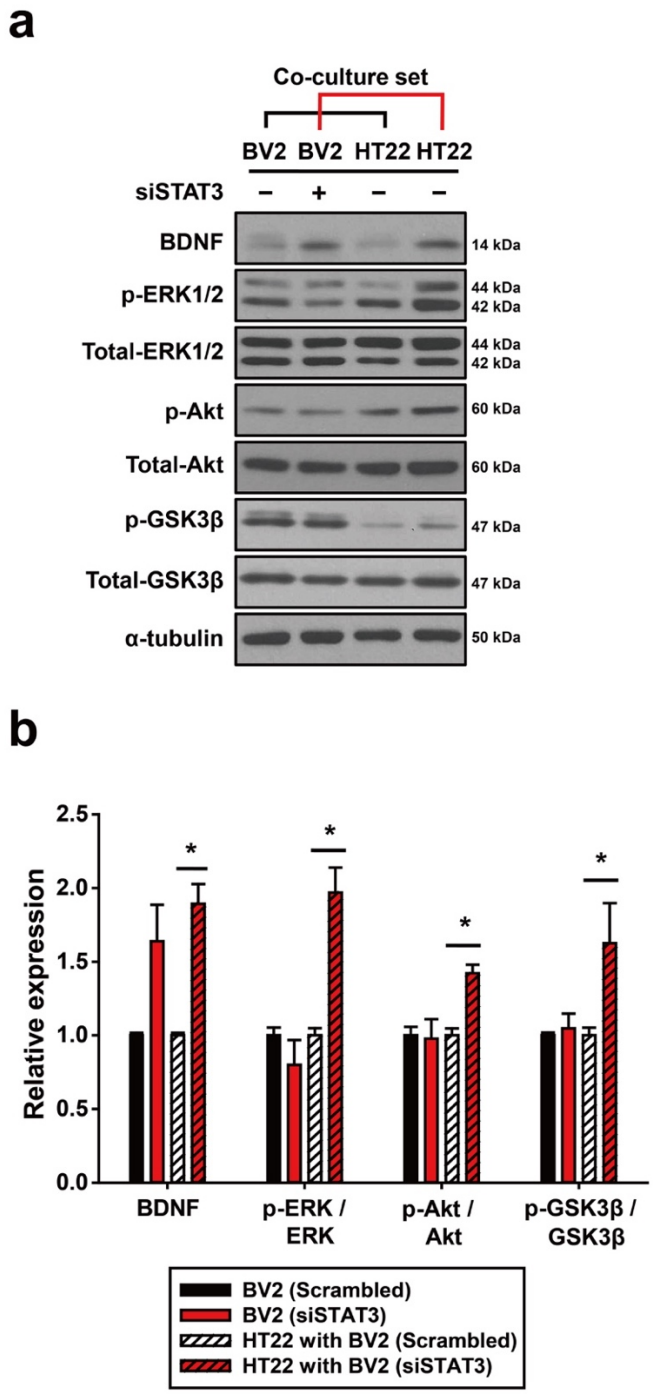
a
Co-culture set
BV2 BV2 HT22 HT22
siSTAT3 – + – –
BDNF
p-ERK1/2
Total-ERK1/2
p-Akt
Total-Akt
p-GSK3β
Total-GSK3β
α-tubulin
14 kDa
44 kDa
42 kDa
44 kDa
42 kDa
60 kDa
60 kDa
47 kDa
47 kDa
50 kDa
b
Relative expression
2.5
2.0
1.5
1.0
0.5
0.0
*
*
*
*
BDNF
p-ERK / ERK
p-Akt / Akt
p-GSK3β / GSK3β
BV2 (Scrambled)
BV2 (siSTAT3)
HT22 with BV2 (Scrambled)
HT22 with BV2 (siSTAT3)

Figure 25. Neuronal M-CSF by interaction with STAT3-deficient microglia triggers the activation of antidepressant signaling pathways.

(a) Western blot analysis of BDNF, ERK1/2, Akt and GSK3β in BV2 and HT22 cells from the co-culture set. (b) Quantification of Western blot was obtained with relative densitometry and normalized with α-tubulin. Data are means ± SEM, and $^{*}p < 0.05$, $^{**}p < 0.01$, $^{***}p < 0.001$. Representative data from three independent experiments are shown.

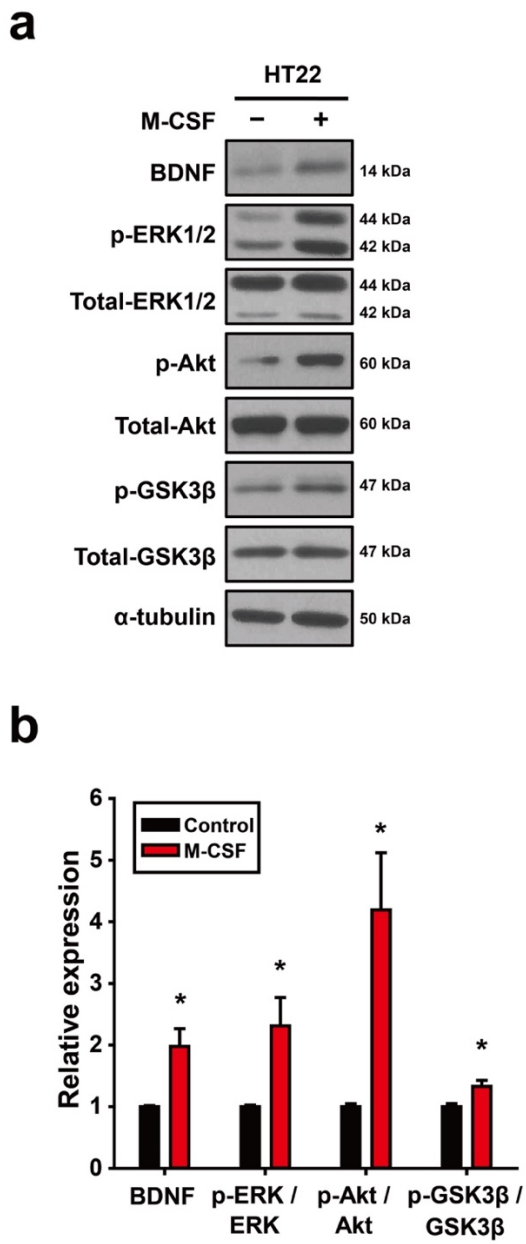
a
HT22
M-CSF
–
+
BDNF
14 kDa
p-ERK1/2
44 kDa
42 kDa
Total-ERK1/2
44 kDa
42 kDa
p-Akt
60 kDa
Total-Akt
60 kDa
p-GSK3β
47 kDa
Total-GSK3β
47 kDa
α-tubulin
50 kDa
b
Relative expression
Control
M-CSF
0
1
2
3
4
5
6
*
BDNF
p-ERK / ERK
p-Akt / Akt
p-GSK3β / GSK3β

Figure 26. M-CSF activates antidepressant signaling pathways in neuronal cell line.

(a) Western blot analysis of BDNF, ERK1/2, Akt and GSK3β in HT22 cells after M-CSF stimulation (40ng/ml) for 24 hours. (b) Quantification of Western blot was obtained with relative densitometry and normalized with α-tubulin. Data are means ± SEM, and *p < 0.05, **p < 0.01, ***p < 0.001. Representative data from three independent experiments are shown.

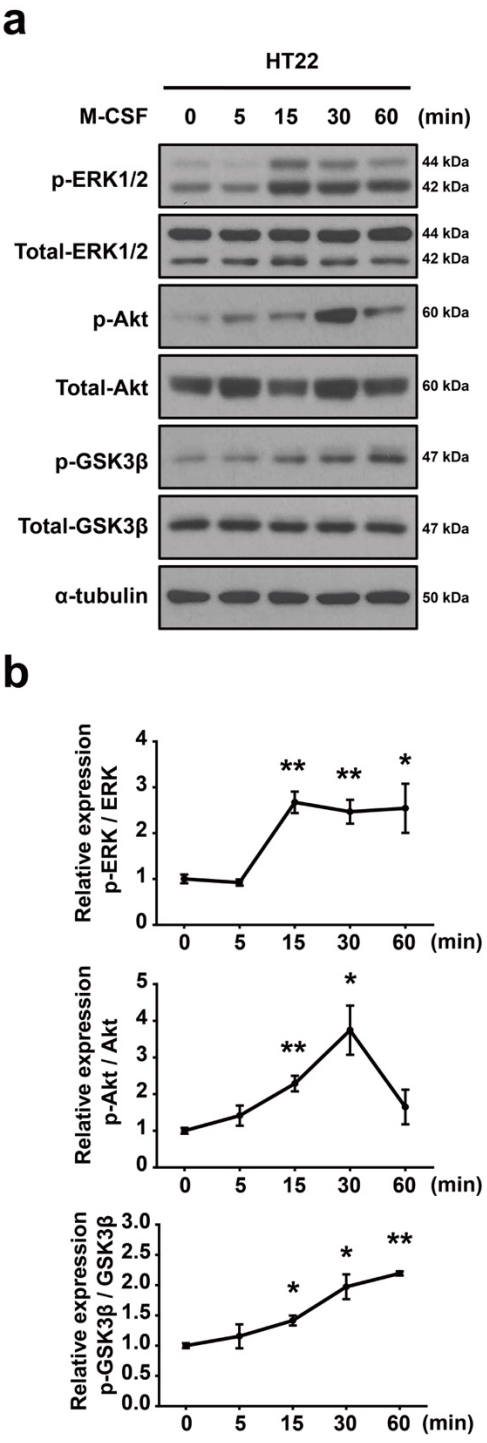
a
HT22
M-CSF 0 5 15 30 60 (min)
p-ERK1/2
Total-ERK1/2
p-Akt
Total-Akt
p-GSK3β
Total-GSK3β
α-tubulin
44 kDa
42 kDa
44 kDa
42 kDa
60 kDa
60 kDa
47 kDa
47 kDa
50 kDa
b
Relative expression p-ERK / ERK
Relative expression p-Akt / Akt
Relative expression p-GSK3β / GSK3β
0 5 15 30 60 (min)

Figure 27. M-CSF activates antidepressant signaling pathways in neuronal cell line.

(a) Western blot analysis of ERK1/2, Akt and GSK3β in HT22 cells after a time-dependent M-CSF (40ng/ml) stimulation. (b) Quantification of Western blot was obtained with relative densitometry and normalized with α-tubulin. Data are means ± SEM, and *p < 0.05, **p < 0.01, ***p < 0.001. Representative data from three independent experiments are shown.

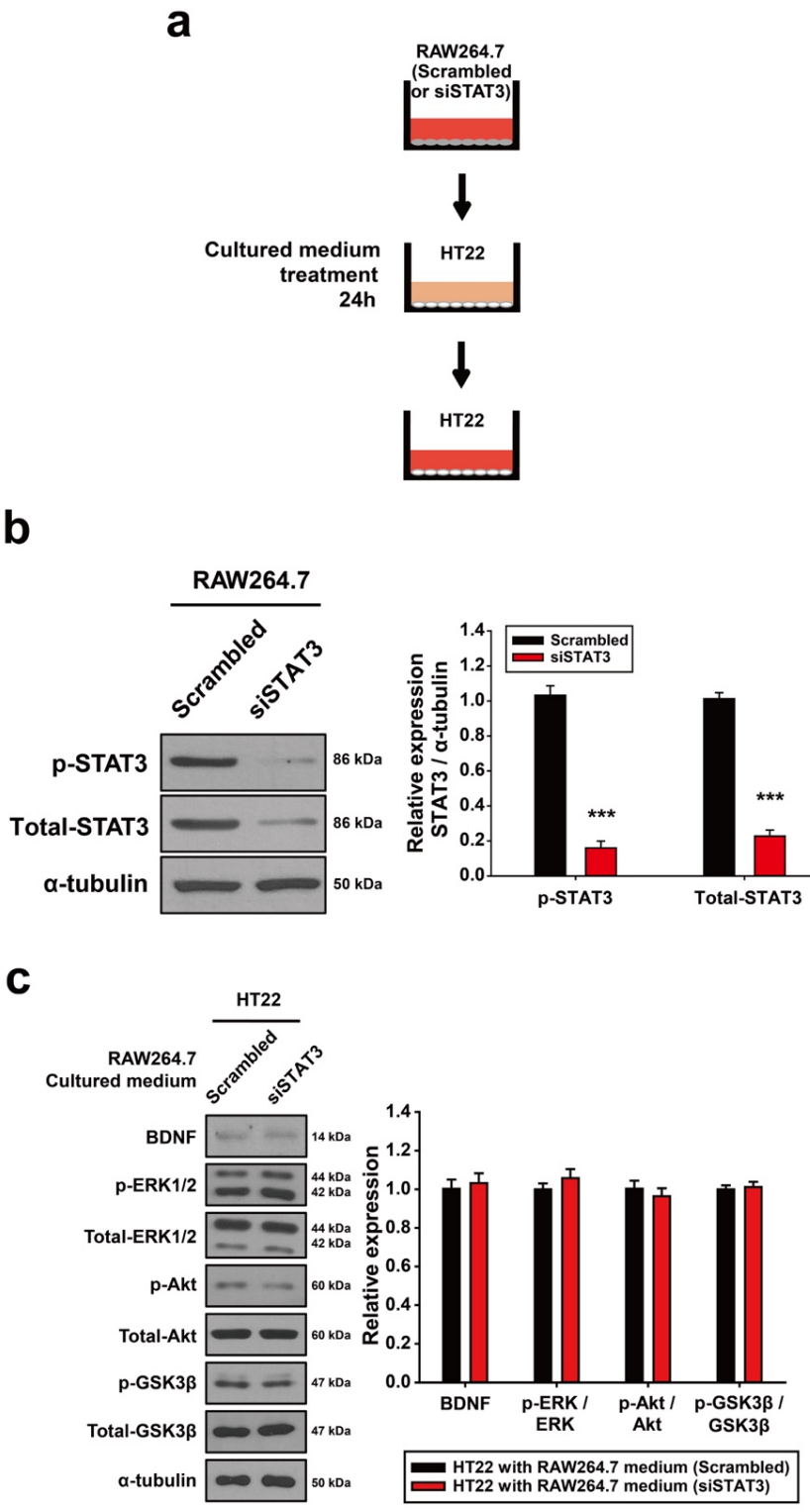
a
RAW264.7
(Scrambled
or siSTAT3)
Cultured medium
treatment
24h
HT22
HT22
b
RAW264.7
Scrambled
siSTAT3
p-STAT3
Total-STAT3
α-tubulin
86 kDa
86 kDa
50 kDa
Relative expression
STAT3 / α-tubulin
Scrambled
siSTAT3
***
***
p-STAT3
Total-STAT3
c
HT22
RAW264.7
Cultured medium
Scrambled
siSTAT3
BDNF
p-ERK1/2
Total-ERK1/2
p-Akt
Total-Akt
p-GSK3β
Total-GSK3β
α-tubulin
14 kDa
44 kDa
42 kDa
44 kDa
42 kDa
60 kDa
60 kDa
47 kDa
47 kDa
50 kDa
Relative expression
BDNF
p-ERK /
ERK
p-Akt /
Akt
p-GSK3β /
GSK3β
HT22 with RAW264.7 medium (Scrambled)
HT22 with RAW264.7 medium (siSTAT3)

Figure 28. Peripheral macrophages have no effect on antidepressant signaling pathways.

(a) Schematic representation of RAW264.7 cultured medium treatments to HT22 cells. (b) Western blot analysis of STAT3 in RAW264.7 cells after scrambled or STAT3 siRNAs transfection. (c) Western blot analysis of BDNF, ERK1/2, Akt and GSK3β in HT22 cells treated with RAW264.7 cultured medium with or without STAT3 inhibition. Each quantification of Western blot was obtained with relative densitometry and normalized with α-tubulin. Data are means ± SEM, and $^{*}p < 0.05$, $^{**}p < 0.01$, $^{***}p < 0.001$. Representative data from three independent experiments are shown.

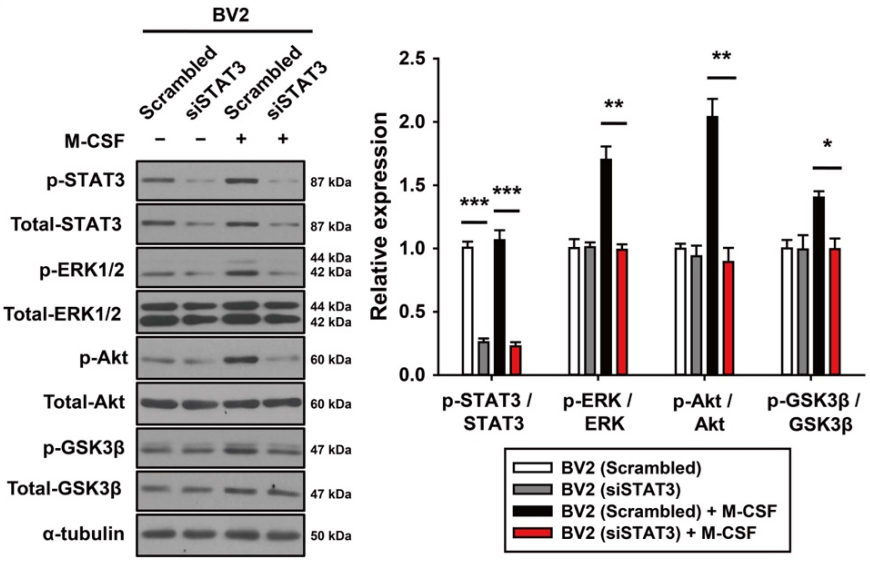

Figure 29. M-CSF has no effect on STAT3-silenced BV2 cells.

Western blot analysis of STAT3, ERK1/2, Akt and GSK3β in BV2 cells after M-CSF (40ng/ml) stimulation for 24 hours with or without inhibition of STAT3 expression. Quantification of Western blot was obtained with relative densitometry, and normalized with α-tubulin. Data are means ± SEM, and *p < 0.05, **p < 0.01, ***p < 0.001. Representative data from three independent experiments are shown.

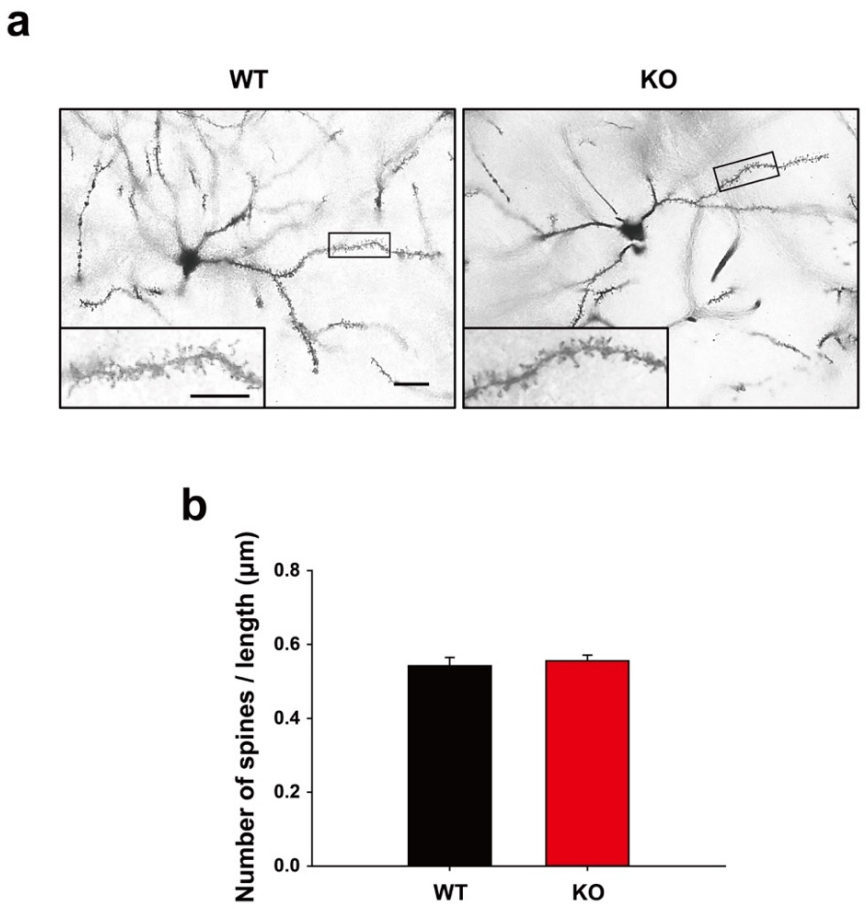

Figure 30. No differences in the number of dendritic spines between the WT and KO mice

(a) Representative images of Golgi staining in the WT and KO groups (n = 5 mice/group). (b) Quantitative data for the number of dendritic spines (0.543 ± 0.022μm vs 0.556 ± 0.015μm in the WT and KO mice, n = 17 and 23 neurons/group, respectively). Scale bar = 40μm. Scale bar of the enlarged image = 20μm.

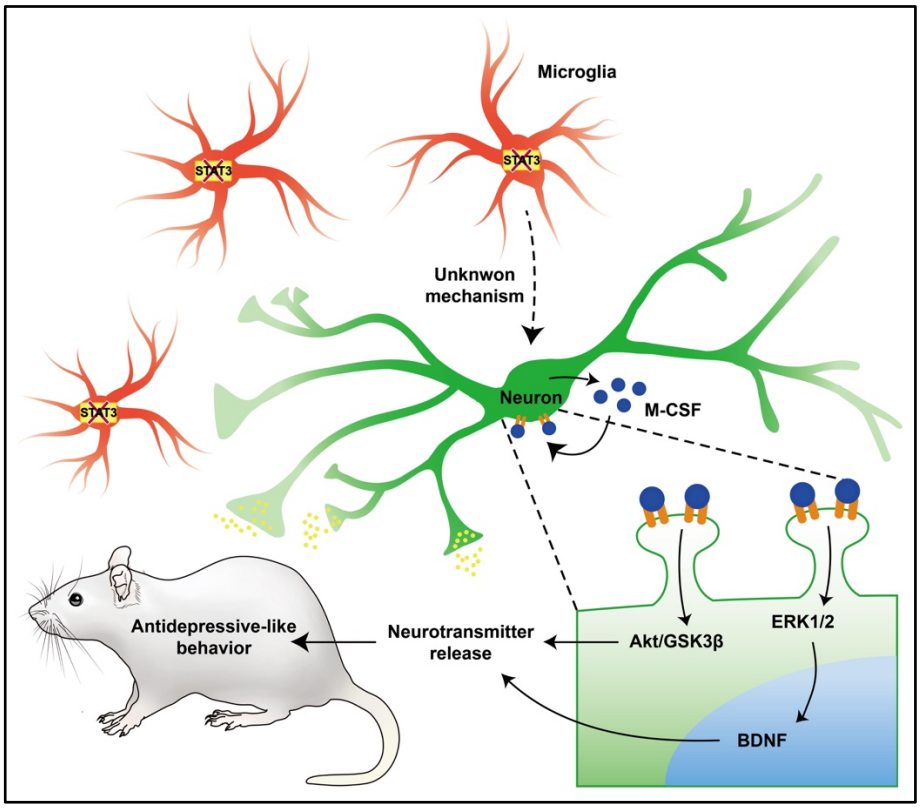
Microglia
STAT3
STAT3
STAT3
Unknwon
mechanism
Neuron
M-CSF
Antidepressive-like
behavior
Neurotransmitter
release
Akt/GSK3β
ERK1/2
BDNF

Figure 31. Dysfunction of STAT3 in microglia enhances M-CSF action on neural functions, and consequently alleviates depression-related behaviors.

Depicted is a schematic model explaining how microglial STAT3 could mediate antidepressant signaling pathways and antidepressive-like behavior in mice. In this model, depletion of STAT3 in microglia initiates its signaling through interacting with neurons, which triggers M-CSF production, leading to the activation of ERK1/2 and Akt/GSK3β through phosphorylation. Enhanced antidepressant signaling pathways and BDNF expression increase neurotransmitter release. Altered synaptic activity could contribute to the modulation of antidepressive-like behavior in mice.

DISCUSSION

In the present study, I explored the mechanisms of neuron–microglia interactions. Primarily, I used a microglia–targeted STAT3–deficient mouse model. From an immunological perspective, STAT3 signaling plays a major role in immune responses, and microglia are CNS–resident immune cells that sense stress in the microenvironment. However, microglia were shown to modulate synaptic activity through functional changes (Wake et al, 2013). In the current study, I demonstrated that dysfunction of STAT3 in microglia enhanced M–CSF action on neural functions along with upregulation of BDNF expression through antidepressant pathways, and consequently alleviated depression–related behaviors (Figure 31). These findings could aid in the development of novel pharmaceutical antidepressant drugs.

My findings on the behavioral association of neuron–microglia interactions show that the STAT3 pathway in microglia may be strongly associated with antidepressive–like behavior. These behavioral experimental results could be categorized as the positive valence system according to Research Domain Criteria (RDoC) for emotional behavior. Despair–based behavior represented by tail suspension and forced swim

tests was responsible for willingness to overcome stressful responses, by measuring motility. Similarly, behavioral processes related to hedonic responses were examined in the sucrose preference test for probing the neural systems for reward seeking behavior. Each experimental design may demonstrate partial aspects of depressive symptoms mimicking human patients' behavior; however, it is quite plausible for newly built criteria on human mental researches.

For many decades, accumulating evidence has reported a positive relationship between depression and cytokines and/or chemokines, such as TNF-α, IL-1, IL-6 and the CC chemokine ligand (CCL) family (Khairova et al, 2009). A recent study suggested that manipulation of the microglia activation status with microglial stimulators, such as lipopolysaccharide (LPS) and M-CSF, could be a potent etiological therapeutics for depression symptomatology (Kreisel et al, 2014). For example, M-CSF could reduce the depressive-like behavior by activating microglia status under chronic stress conditions. In microglial STAT3-deficient model, the microglial STAT3 as a sensor of the cytokine profiles was effectively depleted. Notably, the expression of M-CSF was increased in the brains of $STAT3^{fl/fl}$;$LysM\text{-}Cre^{+/-}$ mice. The elevated mRNA levels and the secretion of M-CSF were detected in neuronal cells in *in vitro* co-culture system. These results implied the novel actions of

M-CSF in the absence of microglial STAT3. Under altered circumstances by deletion of microglial STAT3, M-CSF can be synthesized in neuronal cells and at the same time affect the neuronal cells themselves. For example, M-CSF is produced with an autocrine/paracrine mechanism of action in distinct brain regions, including the dorsal forebrain and cerebellum, and plays an essential role in neural progenitor cell maintenance and maturation (Chitu et al, 2016). In this study, I suggest that M-CSF is involved in autocrine loops in neuronal cells.

Based on these results, I hypothesized that M-CSF actions in neuronal cells could activate certain signaling pathways for antidepressant drugs. In relation to BDNF signaling, I first verified that BDNF expression as well as the phosphorylation of ERK1/2 and Akt/GSK3β was increased in neuronal cells both in STAT3$^{fl/fl}$;LysM-Cre$^{+/-}$ mice and in *in vitro* co-culture system in response to secreted M-CSF. Many studies showed that the ERK1/2 and Akt/GSK3β signaling subsequently induce BDNF expression (Jope et al, 2006; Obata et al, 2003). M-CSF-induced ERK1/2 and Akt/GSK3β signaling pathways potentially work as the molecular mechanisms to regulate antidepressive-like behaviors. Shared with the mechanisms of conventional antidepressant drugs, my findings could be helpful to take less risk for developing novel therapeutics. Thus, these results indicate

that the regulation of ERK1/2 and Akt/GSK3β signaling pathways by M-CSF can be a strong candidate for the development of antidepressants.

Although these results demonstrate the effects of M-CSF on the antidepressant signaling and behavior, further studies are needed to block or inhibit M-CSF signaling in STAT3$^{fl/fl}$;LysM-Cre$^{+/-}$ mice for more clarification. For example, the effect of neutralizing antibodies against M-CSF and blocking anti-mouse M-CSF receptor (known as CSF1R) antibody *in vivo* can be verified using the chronic restrain stress model of STAT3$^{fl/fl}$;LysM-Cre$^{+/-}$ mice. In addition, transgene expression can be restricted to certain cell types using the promoter controlling gene expression in the lentiviral system. Promoters providing specific expression in all neurons include synapsin I (SynI) and neuron specific enolase (NSE). Calcium/calmodulin-dependent protein kinase II alpha (CaMKIIα) also restricts expression to excitatory glutamatergic neurons (Parr-Brownlie *et al*, 2015). Therefore, the induction of depression in STAT3$^{fl/fl}$;LysM-Cre$^{+/-}$ mice using a lentiviral shRNA vector for M-CSF specifically expressed in neurons can effectively demonstrate the relevance of antidepressant signaling pathway.

The data of behavioral analysis showed that microglia-specific STAT3 KO mice had antidepressive-like behavior in both normal and

chronic restraint conditions. This result in normal conditions may be due to changes in the developmental stage of the brain caused by the genetic background of the mouse model. In addition, studies have shown that even without symptoms of depression, antidepressants can be effective in the treatment of depression. For this reason, I have focused on changes in protein expression under normal conditions and have addressed molecular mechanisms. However, in order to understand the more comprehensive function of the microglial STAT3 in depression, it is necessary to identify the molecular mechanism under chronic stress conditions. A recent study showed the quantitative changes of mRNAs in the nucleus accumbens from control, chronic unpredictable mild stress (CUMS)-MDD, and CUMS-resilience mice by high-throughput sequencings (Si *et al*, 2018). The data implicated that the impairment of dopaminergic synapse, circadian process, and calcium signaling may be involved in CUMS-induced depression, whereas the upregulation of tyrosine metabolism, cytokine-cytokine receptor interaction, and calcium signaling may be involved in mouse resilience to the CUMS.

When it comes to neuron-microglia cross-talk, cell-to-cell interactions play a pivotal role in intercellular communication. For example, CX3CR1/CX3CL1 signaling between microglia and neurons is involved in synaptic engulfment, resulted in synaptic elimination (Ueno

et al, 2013; Zhan et al, 2014), and in the modulation of cytokine production and glutamatergic neurotransmission (Rogers et al, 2011; Scianni et al, 2013). CD200 and its receptor, CD200 receptor (CD200R), also have critical roles in the interplay between neurons and microglia by controlling anti-inflammatory signaling and by maintaining them in a resting state (Hoek et al, 2000). Presumably, however, my data indicated that de novo mechanisms of neuron-microglia cross-talk would exist. Ablation of STAT3 in microglia did not alter the number of synaptic dendritic spines. The cytokine array and ELISA experiments also provided that M-CSF production occurs in neuronal cells but not IL-1β, TNF-α, IL-6, and IL-10.

In undertaking this study, I initially hoped to discover unknown targets for neuron-microglia interactions, and investigated the target of microglial STAT3, which increases neuronal M-CSF from the cytokine array. As a target protein of microglial STAT3, CCL2 was treated with neurons to confirm the association with neuronal M-CSF production, but no correlation was found (Figure 18). In fact, it is necessary to neutralize CCL2 to determine the effect on CCL2 reduction and neuronal M-CSF increase for more clear identification. Despite these efforts, there is a limitation in studying the mechanism of interactions between microglia and neurons. One of the major drawbacks of cytokine array in

identifying unknown targets is that only a limited number of proteins can be analyzed. The following methods can be suggested to overcome this. Whole transcriptome sequencing involves large-scale monitoring of relative differences in RNA abundance between experimental groups, which can be used primarily to indicate functional changes. This approach has already gained insights into mechanisms of diseases and biological function, including neuropsychiatric disorders. I also suggest that systematic proteomic analysis can be an alternative approach. A previous study demonstrate that microglial activation occurs the dynamic alteration of the whole cell proteome and secretome. Numerous proteins involved in the immune inflammatory response and metabolism change dynamically as cells are exposed to inflammatory molecules (Woo *et al*, 2017). Analysis of system biology, such as genomics, proteomics, and bioinformatics, will help to broaden understanding of dynamic and complex biological components that are difficult to predict.

As a novel antidepressant mechanism, rapid responses mainly occur through receptor-mediated glutamatergic neurotransmission (Duman et al, 2012b). As previously mentioned, I determined the increase of ERK1/2 and Akt/GSK3β phosphorylation by stimulation of M-CSF. Regarding the ERK1/2 signaling pathways, the release of neurotransmitter was decreased in the inhibition of phosphorylated

ERK1/2 (Kushner et al, 2005). In relation to Akt/GSK3β signaling, the major physiological mechanism that regulates the activity of GSK3 is phosphorylation of GSK3 (Ser9-GSK3β). This serine phosphorylation inhibits the activity of GSK3 and can be catalyzed by Akt (Richard and Myoung-Sun, 2006). Neuronal activation of GSK3β decreases presynaptic glutamate release following high-frequency stimulation and diminishes the expression of SynI, another critical component of the soluble N-ethylmaleimide-sensitive factor attachment protein (SNAP) receptor (SNARE) complex that regulates synaptic vesicle mobilization (Wildburger *et al*, 2012). The GSK3 signaling pathway controls presynaptic transmitter release exerting an overall suppressive effect on synaptic vesicle fusion and neurotransmitter release. Thus, theses evidences implicated that M-CSF-induced ERK1/2 and Akt/GSK3β signaling could enhance the release probability of neurotransmitters, and help elucidate novel antidepressant mechanisms for a rapid-acting antidepressant response.

In conclusion, microglial STAT3 was essential for promoting M-CSF actions on synaptic transmission, which led to antidepressive-like behavior. I propose that ERK1/2 and Akt/GSK3β signaling pathways are involved in BDNF-dependent antidepressant behaviors via M-CSF secretion in neuronal cells. These findings may provide a novel

therapeutic approach for alleviating major depressive disorders.

REFERENCES

Audet MC, Anisman H (2013). Interplay between pro-inflammatory cytokines and growth factors in depressive illnesses. Front Cell Neurosci 7: 68.

Beurel E, Grieco SF, Jope RS (2015). Glycogen synthase kinase-3 (GSK3): Regulation, actions, and diseases. Pharmacology & Therapeutics 148: 114-131.

Brites D, Fernandes A (2015). Neuroinflammation and Depression: Microglia Activation, Extracellular Microvesicles and microRNA Dysregulation. Frontiers in Cellular Neuroscience 9: 476.

Caldeira C, Oliveira AF, Cunha C, Vaz AR, Falcão AS, Fernandes A, et al (2014). Microglia change from a reactive to an age-like phenotype with the time in culture. Frontiers in Cellular Neuroscience 8(152).

Chabot S, Williams G, Yong VW (1997). Microglial production of TNF-alpha is induced by activated T lymphocytes. Involvement of VLA-4 and inhibition by interferonbeta-1b. The Journal of Clinical Investigation 100(3): 604-612.

Chen G, Huang L-D, Jiang Y-M, Manji HK (2000). The Mood-Stabilizing Agent Valproate Inhibits the Activity of Glycogen Synthase Kinase-3. Journal of Neurochemistry 72(3): 1327-1330.

Chitu V, Gokhan **Ş**, Nandi S, Mehler MF, Stanley ER (2016). Emerging Roles for CSF-1 Receptor and its Ligands in the Nervous System. Trends in Neurosciences 39(6): 378-393.

Chuang DM, Wang Z, Chiu CT (2011). GSK-3 as a Target for Lithium-Induced Neuroprotection Against Excitotoxicity in Neuronal Cultures and Animal Models of Ischemic Stroke. Front Mol Neurosci 4: 15.

Cipriani A, Smith K, Burgess S, Carney S, Goodwin G, Geddes J (2006). Lithium versus antidepressants in the long-term treatment of unipolar affective disorder. The Cochrane database of systematic reviews(4): Cd003492.

Clausen BH, Lambertsen KL, Babcock AA, Holm TH, Dagnaes-Hansen F, Finsen B (2008). Interleukin-1beta and tumor necrosis factor-alpha are expressed by different subsets of microglia and macrophages after ischemic stroke in mice. Journal of Neuroinflammation 5(1): 1-18.

Couch Y, Anthony DC, Dolgov O, Revischin A, Festoff B, Santos AI, et al (2013). Microglial activation, increased TNF and SERT expression in

the prefrontal cortex define stress-altered behaviour in mice susceptible to anhedonia. Brain Behav Immun 29: 136-146.

Davis LL, Kabel D, Patel D, Choate AD, Foslien-Nash C, Gurguis GN, et al (1996). Valproate as an antidepressant in major depressive disorder. Psychopharmacology bulletin 32(4): 647-652.

Domino ME, Burns BJ, Silva SG, Kratochvil CJ, Vitiello B, Reinecke MA, et al (2008). Cost-Effectiveness of Treatments for Adolescent Depression: Results From TADS. American Journal of Psychiatry 165(5): 588-596.

Duman RS, Aghajanian GK (2012a). Synaptic Dysfunction in Depression: Potential Therapeutic Targets. Science 338(6103): 68-72.

Duman RS, Aghajanian GK, Sanacora G, Krystal JH (2016). Synaptic plasticity and depression: new insights from stress and rapid-acting antidepressants. Nat Med 22(3): 238-249.

Duman RS, Li N, Liu R-J, Duric V, Aghajanian G (2012b). Signaling Pathways Underlying the Rapid Antidepressant Actions of Ketamine. Neuropharmacology 62(1): 35-41.

Dwivedi Y, Rizavi HS, Conley RR, Pandey GN (2005). ERK MAP kinase signaling in post-mortem brain of suicide subjects: differential regulation

of upstream Raf kinases Raf-1 and B-Raf. Mol Psychiatry 11(1): 86-98.

Dwivedi Y, Rizavi HS, Roberts RC, Conley RC, Tamminga CA, Pandey GN (2001). Reduced activation and expression of ERK1/2 MAP kinase in the post-mortem brain of depressed suicide subjects. Journal of Neurochemistry 77(3): 916-928.

Einat H, Yuan P, Gould TD, Li J, Du J, Zhang L, et al (2003). The Role of the Extracellular Signal-Regulated Kinase Signaling Pathway in Mood Modulation. The Journal of Neuroscience 23(19): 7311-7316.

El Kasmi KC, Holst J, Coffre M, Mielke L, de Pauw A, Lhocine N, et al (2006). General Nature of the STAT3-Activated Anti-Inflammatory Response. The Journal of Immunology 177(11): 7880-7888.

Fang X, Yu SX, Lu Y, Bast RC, Woodgett JR, Mills GB (2000). Phosphorylation and inactivation of glycogen synthase kinase 3 by protein kinase A. Proceedings of the National Academy of Sciences 97(22): 11960-11965.

Felger JC, Lotrich FE (2013). Inflammatory cytokines in depression: neurobiological mechanisms and therapeutic implications. Neuroscience 246: 199-229.

Goodyer I, Dubicka B, Wilkinson P, Kelvin R, Roberts C, Byford S, et al (2007). Selective serotonin reuptake inhibitors (SSRIs) and routine specialist care with and without cognitive behaviour therapy in adolescents with major depression: randomised controlled trial. BMJ 335(7611): 142.

Gourley SL, Wu FJ, Kiraly DD, Ploski JE, Kedves AT, Duman RS, et al (2007). Regionally Specific Regulation of ERK MAP Kinase in a Model of Antidepressant-Sensitive Chronic Depression. Biological Psychiatry 63(4): 353-359.

Hetman M, Kanning K, Cavanaugh JE, Xia Z (1999). Neuroprotection by Brain-derived Neurotrophic Factor Is Mediated by Extracellular Signal-regulated Kinase and Phosphatidylinositol 3-Kinase. 274(32): 22569-22580.

Hisaoka K, Takebayashi M, Tsuchioka M, Maeda N, Nakata Y, Yamawaki S (2007). Antidepressants Increase Glial Cell Line-Derived Neurotrophic Factor Production through Monoamine-Independent Activation of Protein Tyrosine Kinase and Extracellular Signal-Regulated Kinase in Glial Cells. Journal of Pharmacology and Experimental Therapeutics 321(1): 148-157.

Hodes GE, Kana V, Menard C, Merad M, Russo SJ (2015). Neuroimmune mechanisms of depression. Nat Neurosci 18(10): 1386-1393.

Hoek RM, Ruuls SR, Murphy CA, Wright GJ, Goddard R, Zurawski SM, et al (2000). Down-Regulation of the Macrophage Lineage Through Interaction with OX2 (CD200). Science 290(5497): 1768-1771.

Imai Y, Kohsaka S (2002). Intracellular signaling in M-CSF-induced microglia activation: Role of Iba1. Glia 40(2): 164-174.

Jope RS, Roh M-S (2006). Glycogen Synthase Kinase-3 (GSK3) in Psychiatric Diseases and Therapeutic Interventions. Current drug targets 7(11): 1421-1434.

Kamat PK, Kalani A, Tyagi N (2014). Method and validation of synaptosomal preparation for isolation of synaptic membrane proteins from rat brain. MethodsX 1: 102-107.

Karege F, Perroud N, Burkhardt S, Schwald M, Ballmann E, La Harpe R, et al (2007). Alteration in kinase activity but not in protein levels of protein kinase B and glycogen synthase kinase-3beta in ventral prefrontal cortex of depressed suicide victims. Biol Psychiatry 61(2): 240-245.

Khairova RA, Machado-Vieira R, Du J, Manji HK (2009). A potential role for pro-inflammatory cytokines in regulating synaptic plasticity in major depressive disorder. Int J Neuropsychopharmacol 12(4): 561-578.

Kreisel T, Frank MG, Licht T, Reshef R, Ben-Menachem-Zidon O, Baratta MV, et al (2014). Dynamic microglial alterations underlie stress-induced depressive-like behavior and suppressed neurogenesis. Mol Psychiatry 19(6): 699-709.

Kushner SA, Elgersma Y, Murphy GG, Jaarsma D, van Woerden GM, Hojjati MR, et al (2005). Modulation of presynaptic plasticity and learning by the H-ras/extracellular signal-regulated kinase/synapsin I signaling pathway. J Neurosci 25(42): 9721-9734.

Lawson LJ, Perry VH, Dri P, Gordon S (1990). Heterogeneity in the distribution and morphology of microglia in the normal adult mouse brain. Neuroscience 39.

Mori T, Miyamoto T, Yoshida H, Asakawa M, Kawasumi M, Kobayashi T, et al (2011). IL-1beta and TNFalpha-initiated IL-6-STAT3 pathway is critical in mediating inflammatory cytokines and RANKL expression in inflammatory arthritis. Int Immunol 23(11): 701-712.

Obata K, Yamanaka H, Dai Y, Tachibana T, Fukuoka T, Tokunaga A, et al (2003). Differential Activation of Extracellular Signal-Regulated Protein Kinase in Primary Afferent Neurons Regulates Brain-Derived Neurotrophic Factor Expression after Peripheral Inflammation and Nerve Injury. The Journal of Neuroscience 23(10): 4117-4126.

Page ME, Detke MJ, Dalvi A, Kirby LG, Lucki I (1999). Serotonergic mediation of the effects of fluoxetine, but not desipramine, in the rat forced swimming test. Psychopharmacology 147(2): 162-167.

Park KH, Lee TH, Kim CW, Kim J (2013). Enhancement of CCL15 Expression and Monocyte Adhesion to Endothelial Cells (ECs) after Hypoxia/Reoxygenation and Induction of ICAM-1 Expression by CCL15 via the JAK2/STAT3 Pathway in ECs. The Journal of Immunology 190(12): 6550-6558.

Parr-Brownlie LC, Bosch-Bouju C, Schoderboeck L, Sizemore RJ, Abraham WC, Hughes SM (2015). Lentiviral vectors as tools to understand central nervous system biology in mammalian model organisms. Frontiers in molecular neuroscience 8: 14-14.

Perry VH, Nicoll JAR, Holmes C (2010). Microglia in neurodegenerative disease. Nature Reviews Neurology 6: 193.

Riazi K, Galic MA, Kuzmiski JB, Ho W, Sharkey KA, Pittman QJ (2008). Microglial activation and TNFα production mediate altered CNS excitability following peripheral inflammation. Proceedings of the National Academy of Sciences 105(44): 17151-17156.

Richard SJ, Myoung-Sun R (2006). Glycogen Synthase Kinase-3 (GSK3) in Psychiatric Diseases and Therapeutic Interventions. Current Drug Targets 7(11): 1421-1434.

Riley JK, Takeda K, Akira S, Schreiber RD (1999). Interleukin-10 Receptor Signaling through the JAK-STAT Pathway: REQUIREMENT FOR TWO DISTINCT RECEPTOR-DERIVED SIGNALS FOR ANTI-INFLAMMATORY ACTION. Journal of Biological Chemistry 274(23): 16513-16521.

Rogers JT, Morganti JM, Bachstetter AD, Hudson CE, Peters MM, Grimmig BA, et al (2011). CX3CR1 deficiency leads to impairment of hippocampal cognitive function and synaptic plasticity. J Neurosci 31(45): 16241-16250.

Schiepers OJ, Wichers MC, Maes M (2005). Cytokines and major depression. Prog Neuropsychopharmacol Biol Psychiatry 29(2): 201-217.

Scianni M, Antonilli L, Chece G, Cristalli G, Di Castro MA, Limatola C, et al (2013). Fractalkine (CX3CL1) enhances hippocampal N-methyl-d-aspartate receptor (NMDAR) function via d-serine and adenosine receptor type A2 (A2AR) activity. Journal of Neuroinflammation 10(1): 876.

Si Y, Song Z, Sun X, Wang J-H (2018). microRNA and mRNA profiles in nucleus accumbens underlying depression versus resilience in response to chronic stress. American Journal of Medical Genetics Part B: Neuropsychiatric Genetics 177(6): 563-579.

Steiner J, Walter M, Gos T, Guillemin GJ, Bernstein H-G, Sarnyai Z, et al (2011). Severe depression is associated with increased microglial quinolinic acid in subregions of the anterior cingulate gyrus: Evidence for an immune-modulated glutamatergic neurotransmission? Journal of Neuroinflammation 8(1): 1-9.

Streit WJ, Mrak RE, Griffin WST (2004). Microglia and neuroinflammation: a pathological perspective. Journal of Neuroinflammation 1(1): 1-4.

Strekalova T, Spanagel R, Bartsch D, Henn FA, Gass P (2004). Stress-Induced Anhedonia in Mice is Associated with Deficits in Forced Swimming and Exploration. Neuropsychopharmacology 29(11): 2007-

2017.

Tardito D, Perez J, Tiraboschi E, Musazzi L, Racagni G, Popoli M (2006). Signaling Pathways Regulating Gene Expression, Neuroplasticity, and Neurotrophic Mechanisms in the Action of Antidepressants: A Critical Overview. Pharmacological Reviews 58(1): 115-134.

Ueno M, Fujita Y, Tanaka T, Nakamura Y, Kikuta J, Ishii M, et al (2013). Layer V cortical neurons require microglial support for survival during postnatal development. Nat Neurosci 16(5): 543-551.

Wake H, Moorhouse AJ, Miyamoto A, Nabekura J (2013). Microglia: actively surveying and shaping neuronal circuit structure and function. Trends Neurosci 36(4): 209-217.

Wildburger NC, Laezza F (2012). Control of neuronal ion channel function by glycogen synthase kinase-3: new prospective for an old kinase. Frontiers in molecular neuroscience 5: 80-80.

Woo J, Han D, Wang JI, Park J, Kim H, Kim Y (2017). Quantitative Proteomics Reveals Temporal Proteomic Changes in Signaling Pathways during BV2 Mouse Microglial Cell Activation. Journal of Proteome Research 16(9): 3419-3432.

Yirmiya R, Goshen I (2011). Immune modulation of learning, memory, neural plasticity and neurogenesis. Brain, Behavior, and Immunity 25(2): 181-213.

Yu H, Chen Z-y (2011). The role of BDNF in depression on the basis of its location in the neural circuitry. Acta pharmacologica Sinica 32(1): 3-11.

Zhan Y, Paolicelli RC, Sforazzini F, Weinhard L, Bolasco G, Pagani F, et al (2014). Deficient neuron-microglia signaling results in impaired functional brain connectivity and social behavior. Nat Neurosci 17(3): 400-406.

국문 초록

미세아교세포는 중추신경계에 존재하는 신경아교세포계의 한 종류로 뇌와 척수의 신경기능을 보조하거나 보호하는 기능을 한다. 특히, 신경-미세아교세포의 상호작용은 신경-면역계를 정상적으로 유지하는 대표적인 기전 중 하나로 알려져 있으며, 미아교세포의 활성화 상태를 조절하는 것은 신경-면역계의 균형을 유지하는데 매우 중요하다. 신경-면역계의 불균형은 곧 알츠하이머병, 파킨슨병, 주요우울장애 등 여러 신경정신질환의 원인이 되기도 한다. 하지만 신경-미세아교세포의 상호작용이 이러한 신경정신질환에서 어떤 기능을 하는지는 알려져 있지 않다. 신호변환 및 전사활성인자 3 (STAT3)는 일반적으로 면역세포에서 다양한 사이토카인과 성장인자들에 의해 발현되고, 세포 활성화를 일으켜 염증성반응을 일으키는 역할을 유전자이다. 이 연구에서는 미세아교세포-특이적 STAT3 결손이 주요우울장애같은 신경정신질환에서 신경-미세아교세포의 상호작용을 통해 신경면역계의 균형을 유지하고 증상을 완화시킬 것이라는 가설을 세워 연구를 진행했다. 먼저, 미세아교세포-특이적 STAT3 결손 ($STAT3^{fl/fl}$;LysM-$Cre^{+/-}$) 마우스 모델 제작하여 미세아교세포의 STAT3 유전자 활성을 억제시켰고, 장기간의 스트레스로 우울증을 유도한 후 행동분석실험인 강제 수영, 꼬리 매달리기, 자당 선호 및 오픈 필드 테스트를 수행하여 항우울 유사 행동을 보임을 확인했다. 흥미로운 점은 STAT3가 결손된

미세아교세포가 주변의 신경세포와 상호작용을 하여 신경세포로부터 대식세포 콜로니-자극인자 (M-CSF)의 분비를 증가시켰다는 것이다. 상호작용을 한 신경세포는 M-CSF를 자가분비하여 항우울 신호전달경로로 알려진 ERK1/2, Akt/GSK3β가 활성화 되었고, 뇌-유래 신경성장인자 (BDNF) 발현이 증가되었다. ERK1/2, Akt/GSK3β의 활성화와 BDNF 단백질의 신경세포에서의 기능은 신경전달물질의 방출을 증가시키는 것으로 잘 알려져 있으며, 이는 곧 마우스 모델에서 보여준 항우울 유사 행동을 설명할 수 있는 근거가 된다. 결론적으로, 미세아교세포 STAT3의 기능 장애는 M-CSF에 의해 매개된 신경세포 활성을 통해 우울증 관련 행동을 조절하며, 미세아교세포 특이적인 STAT3 기능 억제는 기존의 우울증 치료가 갖고있는 한계점을 극복 할 수 있는 새로운 치료 전략이 될 수 있음을 시사한다.

주요어: 신경세포, 미세아교세포, 신호변환 및 전사활성인자 3 (STAT3), 대식세포 콜로니-자극인자 (M-CSF), 신경-미세아교세포의 상호작용, 신경-면역계, 주요우울장애

학 번 : 2013-21765